Thesis Proposal

Electromagnetic Ion Cyclotron (EMIC) Waves for Radiation Belt Remediation Applications

Maria de Soria-Santacruz Pich

Ph.D Candidate - Aero/Astro Department

Massachusetts Institute of Technology

Submitted: March 26th, 2012

Defense: April 9th, 2012

Committee: Manuel Martinez-Sanchez (supervisor), Gregory Ginet, David Miller, Jeffrey Hoffman and Kerri Cahoy

Abstract

The high energy particles of the Van Allen belts coming from cosmic rays, solar storms, high altitude nuclear explosions (HANEs) and other processes represent a significant danger to humans and spacecraft operating in those regions, as well as an obstacle to exploration and development of space technologies. The "Radiation Belt Remediation" (RBR) concept has been proposed as a way to solve this problem through ULF/VLF transmissions in the magnetosphere, which will create a pitch-angle scattering of these energetic particles. A portion of the particles would then fall into their loss cone, lowering the altitude of their mirror point to a level where they are absorbed by the atmosphere.

The possible utilization of Whistler waves for precipitation of high-energy trapped electrons has been studied extensively [54], and a space test of a linear antenna for this purpose is in preparation [39]. The lower frequency EMIC band has also been studied in the context of electron precipitation [8], but much less work has been devoted to the use of the left-hand polarized branch of EMIC waves for ion precipitation. My thesis focuses on four interconnected research efforts in this direction, which are (1) the radiation of EMIC waves from a spaceborne antenna, (2) their propagation along the Van Allen belts, (3) their interaction with the high-energy particles and (4) the characterization in terms of power, frequency, voltage and current of the RBR transmitter capable of significantly reduce the energetic radiation in the belts. This proposal summarizes the formulation and methodology required to develop these coupled studies as well as the results obtained so far.

The radiation of this frequency band is a broad unexplored territory that should be addressed given its potential practical importance. In my thesis, I will propose solutions to this problem and determine their feasibility. The sheath around a space-based RBR antenna is very thick, and so its capacitance is almost the vacuum capacitance, which is nearly independent of the frequency and proportional to the transmitter length. The associated reactance is extremely high for the EMIC band to the point that it is not possible to use an electric dipole to radiate these waves without the help of any other device. On the other hand, in terms of the radiation resistance, a short antenna would be ideal, because the relevant wavelengths (those near the resonance cone) are indeed very short; unfortunately, short antennas suffer the most from the small capacitance problem, although even a multi-km antenna would have too much reactance at the EMIC regime. In my thesis I will discuss two innovative ways to emit these waves; the first option involves plasma contactors at both ends of a linear dipole, thus avoiding oscillatory charge accumulation. The second case under consideration consists of a magnetic dipole working as an EMIC transmitter. Once the emitter's radiation pattern has been estimated, the propagation of the EMIC mode along the belts would involve ray-tracing of the wave power, which is an input to the wave-particle interaction problem. This last model uses a Lagrangian formulation involving a test particle simulation of the nonlinear equations of motion [56] to reproduce the interaction between the distribution of energetic particles and EMIC waves. This formulation allows one to deal with coherent and narrow-band waves, which are fundamentally different from those produced by incoherent signals. In the later case the particles perform a random walk in velocity space, whereas during the interaction with a coherent wave individual particles are not scattered randomly, but they stay in resonance long enough for the particle's pitch angle to be substantially changed through non-linear interactions. This model will take into account the oblique propagation of coherent EMIC pulsed waves in a multi-ion plasma and their interaction with the energetic protons and electrons in the Van Allen belts.

Contents

List of Figures

Chapter 1

Introduction

1.1 Motivation

The high-energy particles of the Van Allen belts coming from cosmic rays, solar storms, High Altitude Nuclear Explosions (HANEs) and other processes represent a significant danger to humans and spacecraft operating in those regions, as well as an obstacle to exploration and development of space technologies. The emission of ULF and VLF waves from orbiting antennae is a problem of growing interest to the scientific, engineering and defense community, largely motivated by their potential application for artificial modification of the high-energy particle radiation environment, both natural and man-made. These emissions will create a pitch-angle scattering of the energetic particles, causing a portion of them to precipitate into the atmosphere. Despite their strong effects on orbiting spacecraft [14, 13], the total energy residing in these high-energy populations is relatively small, and this opens up the possibility for intervention.

Since the discovery of the radiation belts by Van Allen [113], lots of effort has been dedicated to study the source and loss mechanisms of the high-energy particles that populate the belts. The preponderant effect of high-altitude nuclear explosions is the injection of energetic electrons [21, 85, 90], and so initial research efforts on mitigation techniques have been directed to this component of the trapped radiation. HANEs were carried out to study the injections of electrons in the geomagnetic field even before the discovery of the belts; three of them were conducted under Operation Argus and were confirmed by the satellite Explorer IV in 1958. Later, the "Starfish Prime" HANE was conducted by the US in the central Pacific Ocean in 1962. Starfish generated an artificial belt of trapped energetic electrons over a wide range of L-shells, and damaged three out of five satellites operating at that time.

On the other hand, it is well known that geomagnetic storms cause large-scale injections of both

protons and electrons into the belts, which can increase the quiet-time fluxes by more than two orders of magnitude. The naturally occurring radiation belts, which by themselves constitute a large hazard to spacecraft over an enormous volume of space, contain both electrons and ions (protons mainly), with similar deleterious effects.

Recent studies [1] have concluded that wave-particle interactions may dominate the losses of these energetic particles, suggesting man-made control of the Van Allen belts. Since then, the Whistler-type radiation (between the lower hybrid frequency and the electron gyrofrequency, typically in the tens of kHz) has been studied extensively for precipitation of high-energy trapped electrons, and a space test of a linear antenna for this purpose is in preparation [39]. However, Whistler waves are not capable to interact with the very energetic trapped ions; instead, the proper radiation type would be that of Electromagnetic Ion Cyclotron (EMIC) waves, below the ion gyrofrequency, and hence in the ELF or ULF bands (around 100 Hz). The lower frequency EMIC band has also been studied in the context of electron precipitation [6, 8, 40, 75, 84, 106], but much less study has been devoted to the use of the left-hand polarized branch of EMIC waves for ion precipitation. EMIC spaceborne antennae able to interact with both populations of charged particles is the object of concern to this study.

1.2 Scientific Background

1.2.1 The Magnetosphere

The magnetosphere is the region of space where the plasma is controlled by the geomagnetic field, which is distorted by the plasma ejected outward from the Sun, i.e. the solar wind. The shape of the Earth's magnetosphere is shown in Figure 1.1. The solar wind compresses the dipole field on the sun side and generates a tail (known as magnetotail) in the night side. The boundary created by this effect is known as magnetopause, which is located around $L \approx 10$ ($L = R/R_E$) on the day side and stretches to $L > 60$ on the tail side. Another boundary, the plasmapause, separates the "frozen in" plasma corotating with the Earth from the convecting plasma due to the constant streaming of particles from the solar wind. The location of the plasmapause is strongly influenced by the geomagnetic activity and it varies between $L \approx 3 - 7$. This work focuses in the inner magnetosphere ($L < 7$) , where the Earth's magnetic field can be accurately modeled as a dipole (see Chapter 3). In this region, the bulk plasma can be considered cold and collisionless, with temperatures of $T_e < 1\,eV$ and densities of $n_e = 10^2 - 10^4\,el/cm^3$.

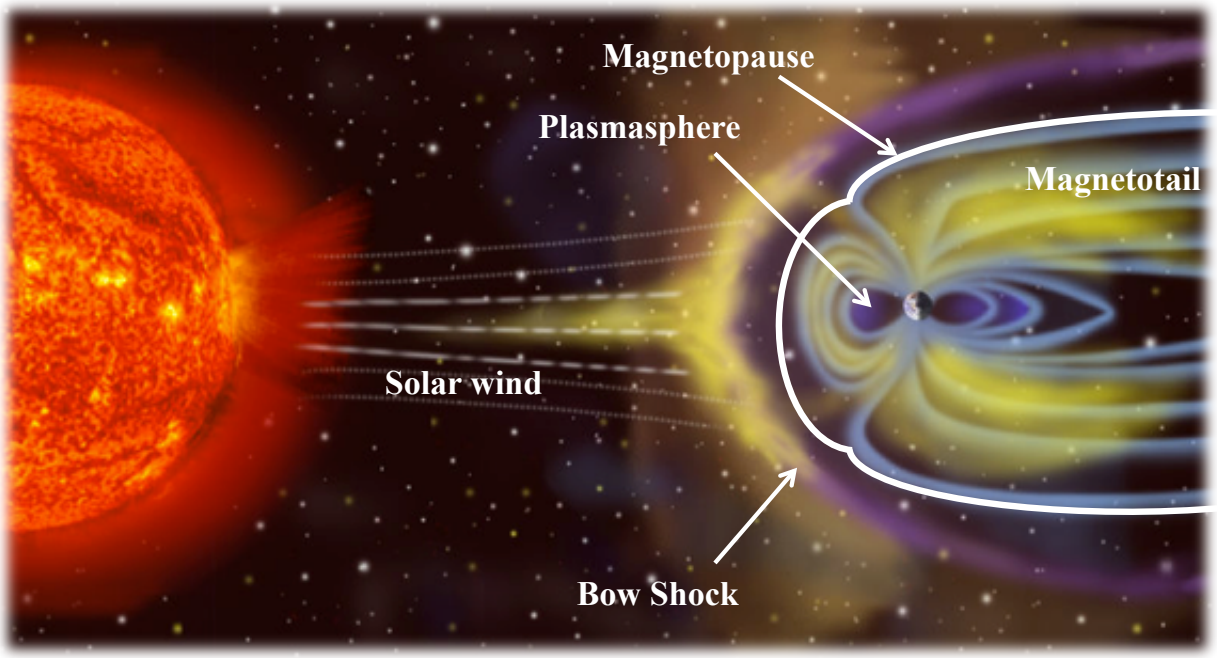

Figure 1.1: Schematic of the magnetosphere.

1.2.2 The Van Allen Belts and the RBR

The Van Allen radiation belts are concentrations of high-energy charged particles generated by cosmic rays, solar storms, and other processes that are trapped in the plasmasphere by the magnetic bottle configuration formed by the Earth's magnetic field. High altitude nuclear explosions (HANEs) would inject as well large amount of energetic electrons into the radiation belts. These particles bounce rapidly back and forth between mirror points above the Earth's atmosphere. The altitude of the mirror point of a particle depends upon the pitch angle of their velocity vector with respect to the magnetic field line. Only those particles with pitch angles greater than a certain level are trapped, while particles with lower pitch angles get lost through the atmosphere because its mirror point falls within a denser region where collisions with atmospheric species effectively remove the particles from the magnetic bottle configuration. Prior to the Space Age, the possibility of trapped charged particles had been investigated by Kristian Birkeland, Carl Størmer and Nicholas Christofilos. The existence of the belt was confirmed by the Explorer 1 and Explorer 3 missions in 1958, under Dr James Van Allen at the University of Iowa [113].

The density of this hot population is very low ($< 1\, el/cm^3$) and they concentrate into two major belts, which are depicted in Figure 1.2: a broad inner belt at $L \approx 1 - 2$ with energies up to 400 MeV for

protons and 1 MeV for electrons [97], and an outer electron belt at $L \approx 3 - 5$ with energies around 0.1-10 MeV. The belts are confined to an area which extends about 65° from the celestial equator. The existence of a safe-gap between the inner and outer belts indicates that there are certain L-shells that do not trap significant amount of electrons of any energy for long periods of time or, equivalently, that there are precipitation mechanisms that are stronger there, probably due to some resonant effects. In addition, the belts contain lesser amounts of other nuclei, such as alpha particles. There is as well the low-energy and quasi-neutral background plasma, with much higher density but lower energy.

The radiation from the belts represents a significant danger to humans and spacecraft operating in those regions, as well as an impediment to exploration and development of space. The high fluxes of energetic particles in the radiation belts will rapidly damage electronic and biological systems. The presence of the high radiation fluxes in the Van Allen belts limits long-duration manned missions to operation below 1200 km of altitude. Shielding to protect against this radiation would be extremely expensive and, even with hardening measures, the lifetime and reliability of space systems will be limited by degradation caused by the trapped particles. Abel and Thorne [1] showed that wave-particle interactions caused by VLF transmissions may dominate losses in the radiation belts. This fact suggested that it could be possible to have practical human control on the belts to protect the systems orbiting the Earth from natural or HANEs injections. This idea of controlled removal of high-energy particles was named Radiation Belt Remediation (RBR) [94]. Some approaches to the RBR use spaceborne antennas to inject ULF/VLF waves into the belts that scatter the energetic particles and precipitate them [39, 87], which is the purpose of the present work.

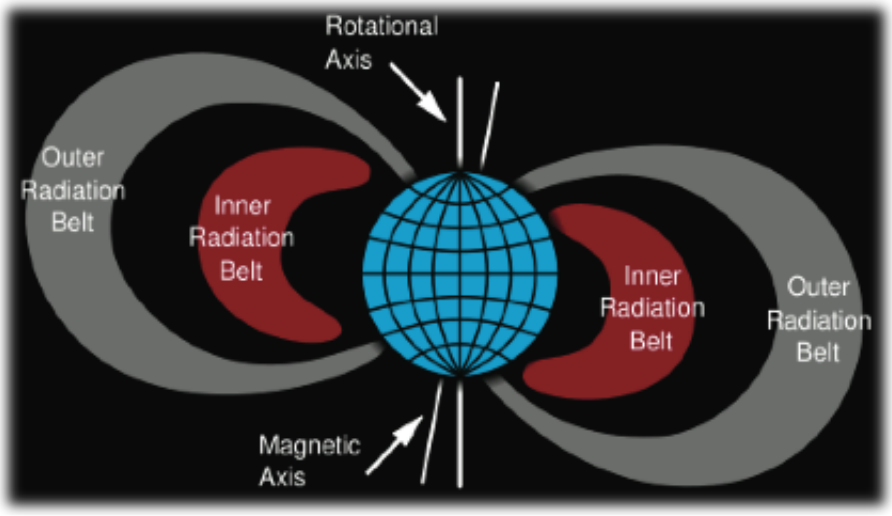

Figure 1.2: Schematic of the Van Allen Belts

1.2.3 Dynamics of the Trapped Particles

The high-energy particles trapped in the belts perform three basic motions: gyro-motion around the magnetic lines, bouncing motion along them and drift motion around the Earth, as schematized in Figure 1.3. When the variation of the magnetic field with position and time is sufficiently slow, there is and adiabatic invariant associated with each of these motions, which is the action integral associated with each of the periodicities. Each invariant is really the leading term in an asymptotic series in a smallness parameter, but in this study we will only consider invariance to the lowest order, which is widely used to explain the charged-particle motion in the Van Allen or artificial belts; the derivation of the higher order terms can be found elsewhere [43]. These conservation laws lead to retention of the particles in the field. Even though the Earth's magnetic field is far from symmetric with respect to any axis, it can be shown [89] that for a quiescent magnetosphere, long trapping times are to be expected. Recently, Selesnick et al. [97] developed a theoretical model of the high-energy particles in the inner proton belt and provided proton intensities as a function of time and the three adiabatic invariants.

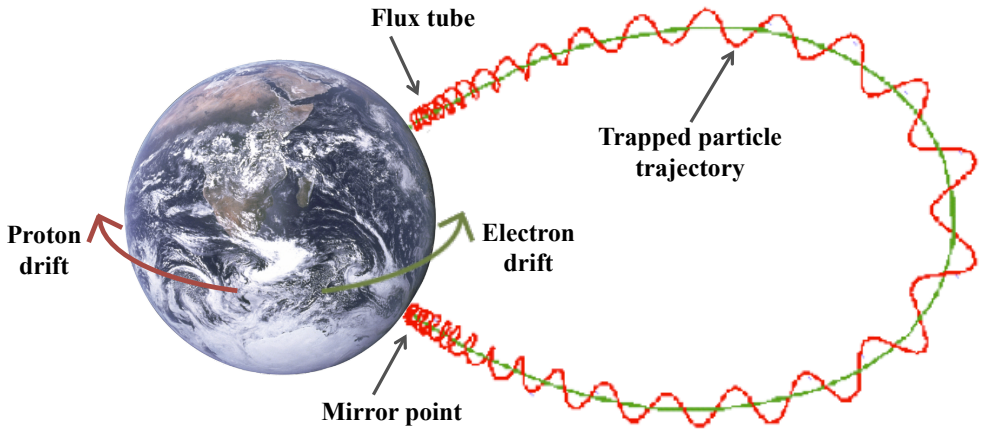

Figure 1.3: Trapped particle motions

In a magnetic field with space and time variations small compared to the radius and period of gyration of the particle, the particle describes approximately a circle with center moving along the line of force and slowly drifting at right angles to that line. The motion along the local $\vec{B}$ field is given by

$$\left\langle \frac{dp_{II}}{dt} \right\rangle = -\frac{\mu}{\gamma}\frac{\partial B}{\partial s} + qE_{II} \tag{1.1}$$

where B and E are magnetic and electric fields, p_{II} and $p_{\perp}$ are the momentum components parallel

and perpendicular to the external magnetic field, $\alpha = atan\left(p_{\perp}/p_{II}\right)$ is the particle's pitch angle, γ is the relativistic factor, s is the distance along the line of force and μ is the magnetic moment given by

$$\mu = \frac{p_{\perp}^2}{2mB} \tag{1.2}$$

The drifting motion that moves the guiding center to a neighboring line is given by

$$\vec{v}_g = \frac{\hat{n}}{B} \times \left(-\vec{E} + \frac{\mu}{\gamma q} \nabla B + \frac{p_{II}^2}{\gamma q m} \frac{\partial \hat{n}}{\partial s} \right) \tag{1.3}$$

where $\hat{n}$ is the unit vector along the Earth's magnetic field vector. The first term in the right side of the equation above is the $\vec{E} \times \vec{B}$ drift, which is in the same direction for both electrons and protons. The second term is the grad-B drift due to the variation of the magnetic field over a gyroperiod, and the third term corresponds to the curvature drift due to the centrifugal force over a particle with parallel velocity v_{II}. This equation is valid if its right hand side is small compared to the velocity of the particle. Grad-B and curvature drifts give an azimuthal current, with electrons moving eastward and positive ions drifting westward. In addition, in the absence of azimuthal symmetry, gradients and curvature components in the azimuthal direction could give drifts in the radial direction.

The magnetic moment μ introduced in Eq. 1.2 constitutes the first adiabatic invariant. The magnetic moment is a conserved quantity in the inner magnetosphere because the high-energy particles have a gyroradius that is much smaller than the variation length-scale of the magnetic field. Invariance of μ implies that the particle will bounce back at the point where the Earth's magnetic field equals $B_{TP} = p^2/\left(2\mu m\right)$, which corresponds to $v_{\parallel TP} = 0$. By conservation of energy $p^2 = p_{\perp}^2 + p_{II}^2$ is constant ($p^2 = 2mE$), and at any point B_0 along a line we have that $B_0 = p_{\perp 0}^2/\left(2\mu m\right)$, thus dividing by B_{TP} we get

$$\frac{B_0}{B_{TP}} = \frac{p_{\perp 0}^2}{p^2} = \frac{p_{\perp 0}^2}{p_0^2} = sin^2\alpha_0 \tag{1.4}$$

This proves that the turning point is independent of momentum and charge of the particle, and only dependent on the pitch angle at a given point along the line, like the equator. In addition, if there is no electric field, the kinetic energy is a constant of the motion and the particle always reflects at the same magnitude of the magnetic field. Eq. 1.2 can be rewritten as follows

$$\frac{p_{\perp}^2}{B} = \frac{p^2 sin^2\alpha}{B} = constant \tag{1.5}$$

which allows to compute the pitch angle at any position of the trajectory, provided B is known at that position. In terms of the equatorial values, the pitch angle can be expressed as follows

$$sin\alpha\,(s) = \sqrt{\frac{B\,(s)}{B_{eq}}} sin\alpha_{eq} \tag{1.6}$$

where s is the distance along the line of force.

If we define B_a as the magnetic field intensity at the border of the sensible atmosphere ($\sim$100 km), particles with $\alpha < \alpha_{lc} = 1/sin\left(\sqrt{B/B_a}\right)$ will be removed from the trapped configuration by collisions in the atmosphere. The pitch angle α_{lc} is called bounce loss cone pitch angle.

Taking into account the asymmetry of the magnetic field, these statements do not lead to the conclusion that a particle drifting around the Earth will return to the starting line of force. However, it can be shown [89] that the time average of this drift conserves the second or longitudinal invariant J, which is given by

$$J = \oint p_{II} ds \tag{1.7}$$

where ds is the element of length of the line of force, and the integral is over a complete oscillation along that line. The second adiabatic invariant of the guiding center motion is associated with the bouncing motion between two mirror points in a magnetic line, and it is only constant provided that the magnetospheric magnetic field and the drift velocity $\vec{v}_g$ vary on time-scales much longer than the bouncing period. Since the bounce time for MeV protons and electrons is a few seconds at most, this is not a particularly demanding constraint. At each longitude there is only one field line between mirror points having the required J, thus in a static field it is true that the particle remains in the same B-shell as long as the second invariant is conserved. In other words, if the kinetic energy and the magnetic moment are constant, the invariance of J prevents charged particles from moving radially in or out of the belts as they rotate around the Earth, which helps to explain their persistence.

However, to study the time-dependent field we need to introduce the third or flux invariant Φ, which is the flux of $\vec{B}$ inside the invariant surface enclosed by the drift path. This invariant is associated with the precession of particles around the Earth, and its rigorous derivation has been proven by Northrop [88]. Φ is only constant provided that the Earth's magnetic field varies on time-scales much longer than the drift period. Since the drift period for MeV protons and electrons is around an hour, this is only likely to be the case when the magnetosphere is relatively quiescent.

According to adiabatic theory and the lowest-order invariants, the energetic particles in the radiation belts would remain indefinitely in the geomagnetic field and continuously precess about their invariant surfaces. Figures 1.4 and 1.5 show omnidirectional fluxes of the trapped protons and electrons, respectively. The AP-8 model by NASA [86] allows the computation of these fluxes for specified energies, L-shells and magnetic field strengths. However, solar wind can produce disturbances that are

sufficiently fast to affect the adiabatic invariants. During magnetic storms, particles will diffuse from one invariant surface to another and may eventually get lost away from the earth or down into the atmosphere. In addition, precipitation induced by wave particle interactions is one of the major loss processes for the radiation belt particles [1]. We must note that if the particle is not trapped between mirrors, the longitudinal motion is not periodic, which means that there is not even a second nor a third adiabatic invariants, but only the magnetic moment exists.

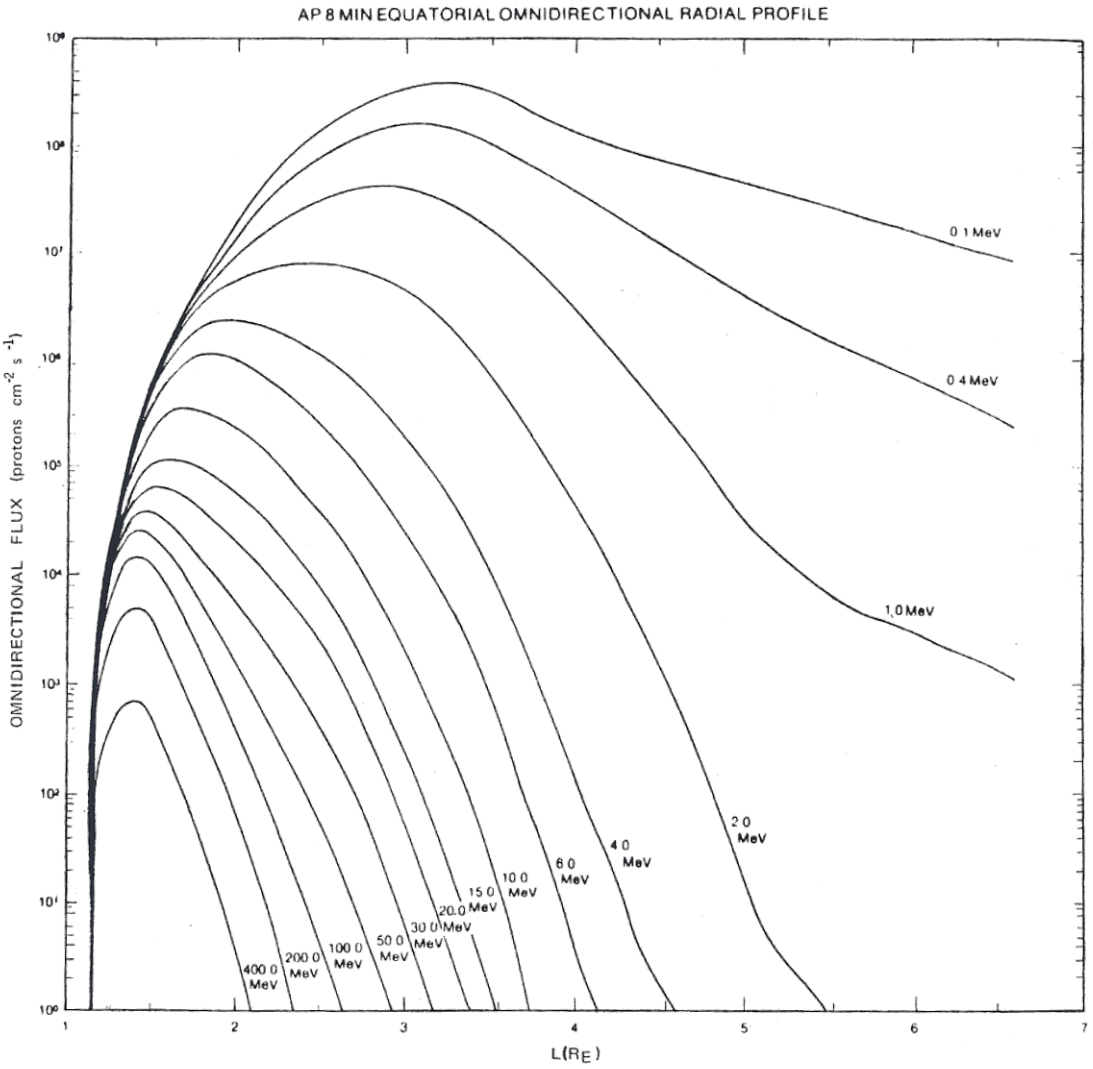

Figure 1.4: Radial distribution of AP8MIN omnidirectional fluxes of protons in the equatorial plane with energies between 0.1 and 400 MeV. [64]

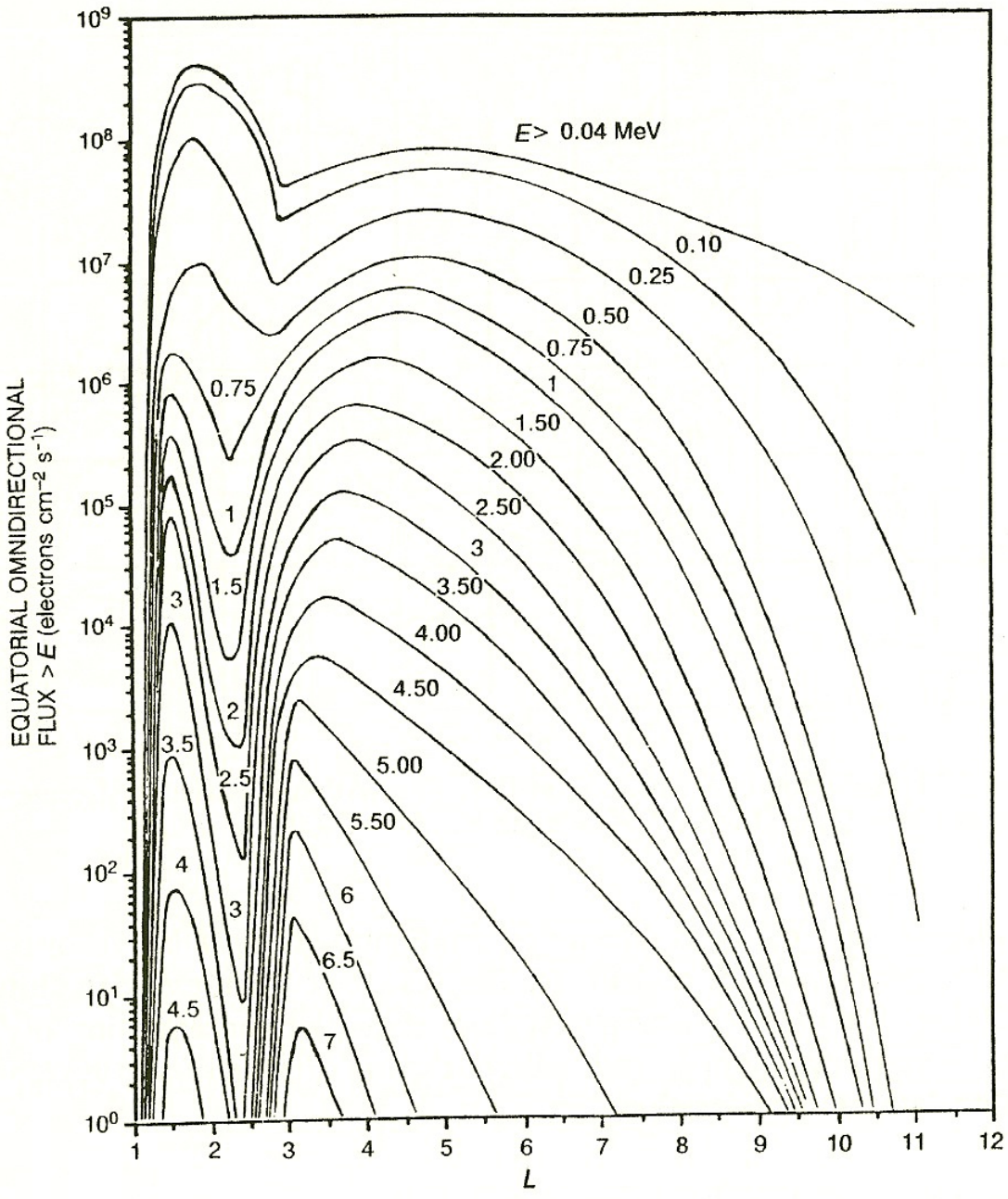

Figure 1.5: Integral, omnidirectional fluxes of electrons in the equatorial plane with energies between 0.1 and 7 MeV. [115]

1.2.4 Electromagnetic Ion Cyclotron Waves

Electromagnetic Ion Cyclotron (EMIC) waves are plasma waves that propagate below the proton gyrofrequency Ω_p, which is given by

$$\omega < \Omega_p = \frac{eB_0}{m_p} \tag{1.8}$$

where e is the electron charge, B_0 is the external magnetic field and m_p is the proton mass. The subscripts p and e denote protons and electrons, respectively.

In this study we use the theory of cold plasma wave propagation as a first approximation. Although the bulk plasma in the magnetosphere is in the thermal range (0.1-10 eV), the topological characteristics of the dispersion relation are not strongly influenced by the ion temperature, but it only leads to small modifications of the phase and group velocities of the wave. Assuming cold plasma waves, the dispersion relationship can be expressed as follows [104]

$$An^4 - Bn^2 + C = 0 \tag{1.9}$$

where $n = c\left|\vec{k}\right|/\omega$ is the index of refraction, $\vec{k}$ is the wavenumber vector, c is the speed of light and

$$A = Ssin^2\theta + Pcos^2\theta \tag{1.10}$$

$$B = RLsin^2\theta + PS\left(1 + cos^2\theta\right) \tag{1.11}$$

$$C = PRL \tag{1.12}$$

where θ is the angle between the external magnetic field and the wave normal direction, and the wave coefficients are given by

$$R = 1 - \sum_l \frac{\omega_{pl}^2}{\omega^2}\frac{\omega}{\omega + \Omega_l} \tag{1.13}$$

$$L = 1 - \sum_l \frac{\omega_{pl}^2}{\omega^2}\frac{\omega}{\omega - \Omega_l} \tag{1.14}$$

$$P = 1 - \sum_l \frac{\omega_{pl}^2}{\omega^2} \tag{1.15}$$

$$S = \frac{R+L}{2} \tag{1.16}$$

$$D = \frac{R-L}{2} \tag{1.17}$$

the summations are over all species including electrons. The plasma frequency ω_{pl}, and the cyclotron frequency Ω_l are defined as follows

$$\omega_{pl} = \sqrt{\frac{q_l^2 n_l}{m_l \epsilon_0}} \tag{1.18}$$

$$\Omega_l = \frac{q_l B_0}{m_l} \tag{1.19}$$

where n_l, m_l and $q_l = Z_l e$ are the density, mass and charge of the l-species, respectively. Rearranging Eq. 1.9 we get

$$n^2 = \frac{2PRL}{(RL-PS)\,sin^2\theta + 2PS \pm \sqrt{(RL-PS)^2\,sin^4\theta + 4P^2D^2cos^2\theta}} \tag{1.20}$$

The sums in Eqs. 1.13 to 1.15 are much larger than one because the frequencies under consideration are such that $\omega/\left|\Omega_e\right| << \omega_{pe}^2/\Omega_e^2$. With this approximation and normalizing with ω_{pe}^2/Ω_e^2, the coefficients can be expressed as [6, 62]

$$\overline{R} = -\frac{1}{MY}\left[\frac{1}{MY-1} + \sum_i \frac{\gamma_i Z_i}{\beta_i Y/Z_i + 1}\right] \tag{1.21}$$

$$\overline{L} = -\frac{1}{MY}\left[\frac{1}{MY+1} + \sum_i \frac{\gamma_i Z_i}{\beta_i Y/Z_i - 1}\right] \tag{1.22}$$

$$\overline{P} = -\left(\frac{1}{MY}\right)^2\left[1 + M\sum_i \frac{\gamma_i Z_i^2}{\beta_i}\right] \tag{1.23}$$

$$\overline{S} = \frac{\overline{R}+\overline{L}}{2} \tag{1.24}$$

$$\overline{D} = \frac{\overline{R}-\overline{L}}{2} \tag{1.25}$$

where the summations are over all ion species and $\gamma_i = n_i/n_e$, $Z_i = q_i/e$, $M = m_e/m_p$, $\beta_i = m_i/m_p$ and $Y = \omega/\Omega_p$. The overbars will be dropped from now on. With these assumptions, the cold plasma dispersion relationship can be expressed as follows

$$n^2 = \frac{\omega_{pe}^2}{\Omega_e^2}\Psi^{-1} \tag{1.26}$$

where

$$\Psi = \frac{(RL - PS)\, sin^2\theta + 2PS \pm \sqrt{(RL - PS)^2\, sin^4\theta + 4P^2D^2cos^2\theta}}{2PRL} \tag{1.27}$$

The sign of Ψ determines two branches of the wave mode, which can be left (L-mode) or right (R-mode) hand polarized. Waves only propagate for $\Psi > 0$. To follow one branch, the sign of Ψ must be changed whenever crossing a cyclotron frequency, or in other words, whenever $L \to \infty$.

From Eq. 1.9 it can be observed that resonances occur whenever $n \to \infty$, which corresponds to $A = 0$, or

$$tan^2\theta_{res} = -P/S \tag{1.28}$$

A very good estimation of these locations is given by

$$Y_{res_i} = \left(\frac{Z_i}{\beta_i}\right)\left[1 + \frac{M}{2}\frac{\gamma_i Z_i^2}{\beta_i} tan^2\theta\right] \tag{1.29}$$

For the particular case of perpendicular propagation ($\theta = 90°$) these resonances correspond to the bi-ion frequencies ($S = 0$), which are mixed resonances between two ion species. At frequencies above the bi-ion frequency, EMIC waves exhibit a resonance cone that prevents them from getting perpendicular to the geomagnetic field, thus wave reflection cannot occur until they propagate to higher latitudes and the local bi-ion frequency increases above the wave frequency [109]. At the bi-ion frequency the wave-normal angle equals $\theta = 90°$, the parallel group velocity is zero and the wave is reflected [91]. For parallel propagation ($\theta = 0$), resonances happen at the cyclotron frequencies of each ion species ($L \to \infty$, $S \to \infty$).

Cutoffs occur whenever $n \to 0$, which corresponds to $RPL = 0$. At the cutoff frequency, reflection of the L-mode occurs and it does not propagate between the cutoff and the resonance frequency of each ion species. A very good estimation of the cutoff frequencies is given by

$$Y_{cf_i} = \frac{1}{4}\left(1 + 3\gamma_i\right) \tag{1.30}$$

We will now analyze the dispersion of the EMIC band in a $H^+ - He^+ - O^+$ plasma. The dispersion characteristics in a $H^+ - He^+$ plasma have been studied by several authors [91, 123], and the propagation of EMIC waves in a $H^+ - He^+ - O^+$ plasma was later studied by Albert [6] and Ludlow [77]. Compared to a proton-electron plasma, the dispersion and propagation characteristics of these waves are dramatically modified in the presence of other heavy ions (O^+ and He^+), which give rise to polarization reversals and spectral slots as we will show next. In a multi-ion plasma it can happen that $D = 0$, which corresponds to crossover frequencies. At the crossover frequencies a particular branch changes from R to L modes through linear polarization, and vice versa. In other words, left and right polarizations of obliquely propagating EMIC waves in a multi-ion plasma are coupled. In the case of parallel propagation, both polarizations are decoupled and the branches intersect each other at the crossover frequencies, but they don't exchange polarization. The following expression gives a very good estimation of the crossover frequencies

$$Y_{cr_i} = \frac{1}{4}\sqrt{1 + 15\gamma_i} \tag{1.31}$$

Figure 1.6 shows the simplest form of the dispersion in an electron-proton plasma for a wave-normal angle of $\theta = 45°$ and varying frequency. We clearly observe the resonance of the guided left-hand branch at $Y = 1$. On the other hand, the unguided right-hand mode remains unaffected by the proton gyrofrequency and propagates though it.

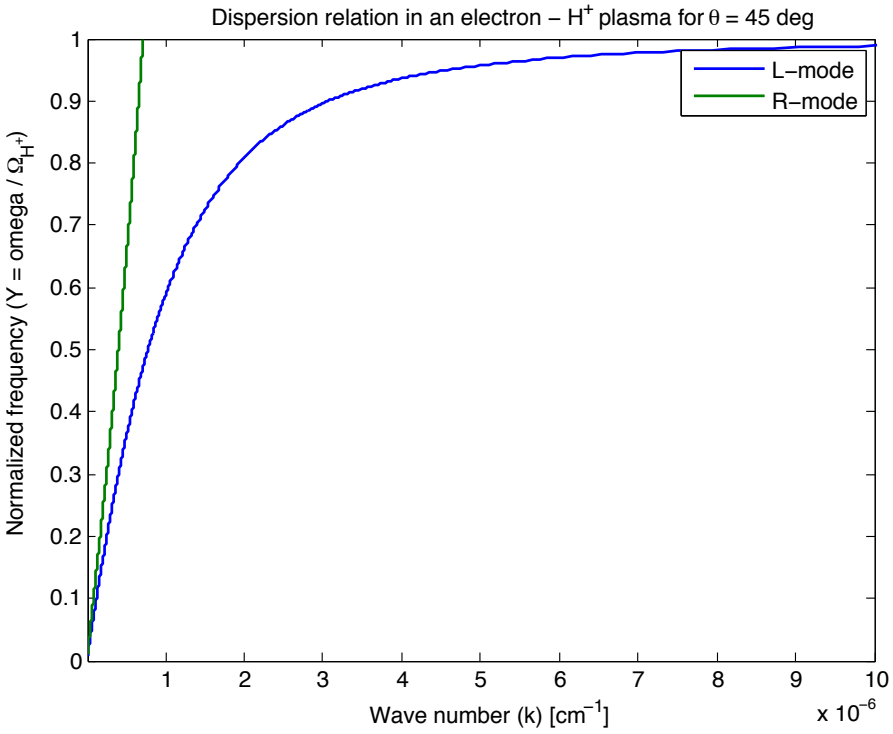

Figure 1.6: Dispersion relation in an electron-proton plasma for $\theta = 45°$.

Consider now the more complicated case of an $H^+ - He^+ - O^+$ plasma with $\gamma_{H^+} = 0.77$, $\gamma_{He^+} = 0.20$ and $\gamma_{O^+} = 0.03$. Figure 1.7 presents the dispersion relation for a wave propagating at $\theta = 45°$ with varying frequency. These dispersion curves are very different compared to the electron-proton case. The left branches resonate at the frequencies given by Eq. 1.28 ($\omega_{res_{O^+}}$ and $\omega_{res_{He^+}}$), and they do not propagate through the stop bands generated between the resonant and cutoff frequencies ($\omega_{cf_{O^+}}$ and $\omega_{cf_{He^+}}$) of each ion species. At the cutoff frequencies a new L branch appears, and both solutions exchange labels at the crossover frequencies. It is important to notice that mode-conversion allows tunneling of these waves through the critical region for the L-mode, which would explain the observations of EMIC waves from ground [34, 47].

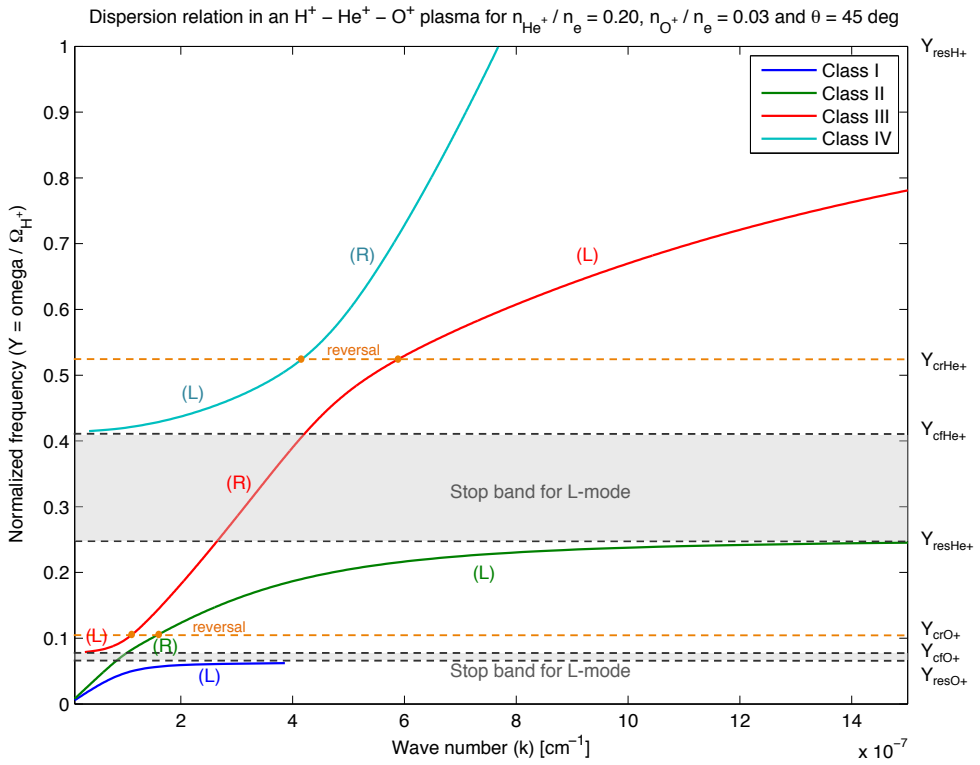

Figure 1.7: Dispersion relation for $\gamma_{H^+} = 0.77$, $\gamma_{He^+} = 0.20$, $\gamma_{O^+} = 0.03$ and $\theta = 45°$.

Figure 1.8 shows the dispersion relation for perpendicular propagation. For $\theta = 90°$ the expression simplifies to X and O-modes [104], which are given by

$$O - mode: \quad n = \frac{\omega_{pe}}{|\Omega_e|}\sqrt{P} \tag{1.32}$$

$$X - mode: \quad n = \frac{\omega_{pe}}{|\Omega_e|}\sqrt{\frac{RL}{S}} \tag{1.33}$$

However, in our range of frequencies $P < 0$, which means that only the X-mode propagates. As described above, the resonances for perpendicular propagation happen at the bi-ion frequencies, which are controlled by the concentration of heavy species.

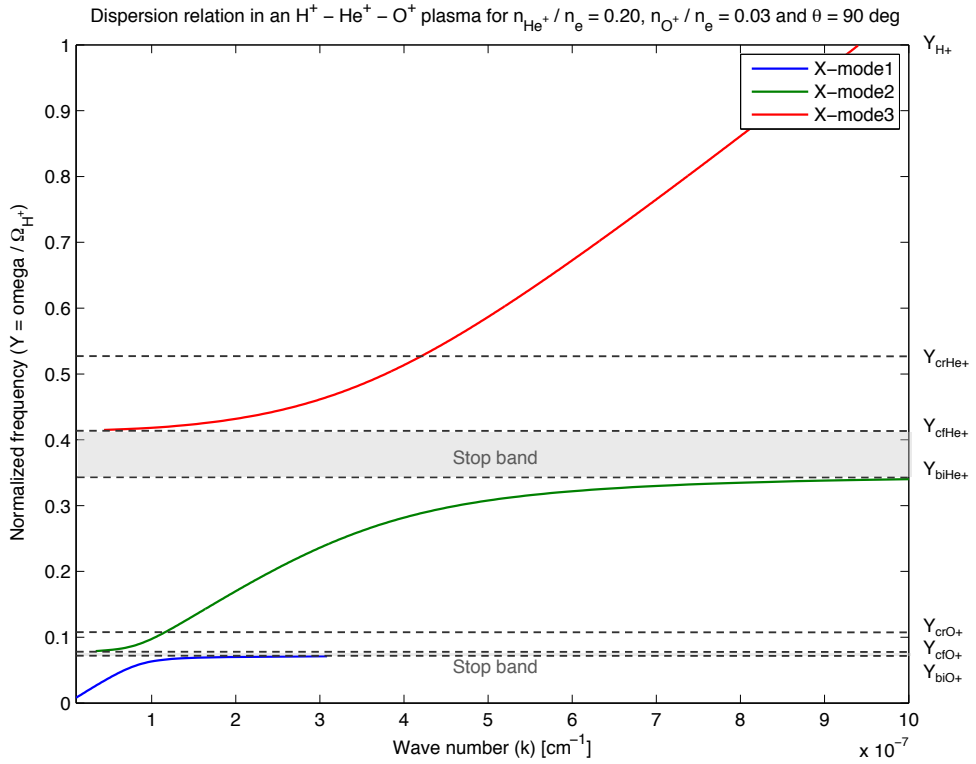

Figure 1.8: Dispersion relation for $\gamma_{H^+} = 0.77$, $\gamma_{He^+} = 0.20$, $\gamma_{O^+} = 0.03$ and $\theta = 90°$.

Finally, Figure 1.9 shows the case of parallel propagation. In this situation, the left and right branches are decoupled and the resonances happen at the cyclotron frequencies of the different ion species.

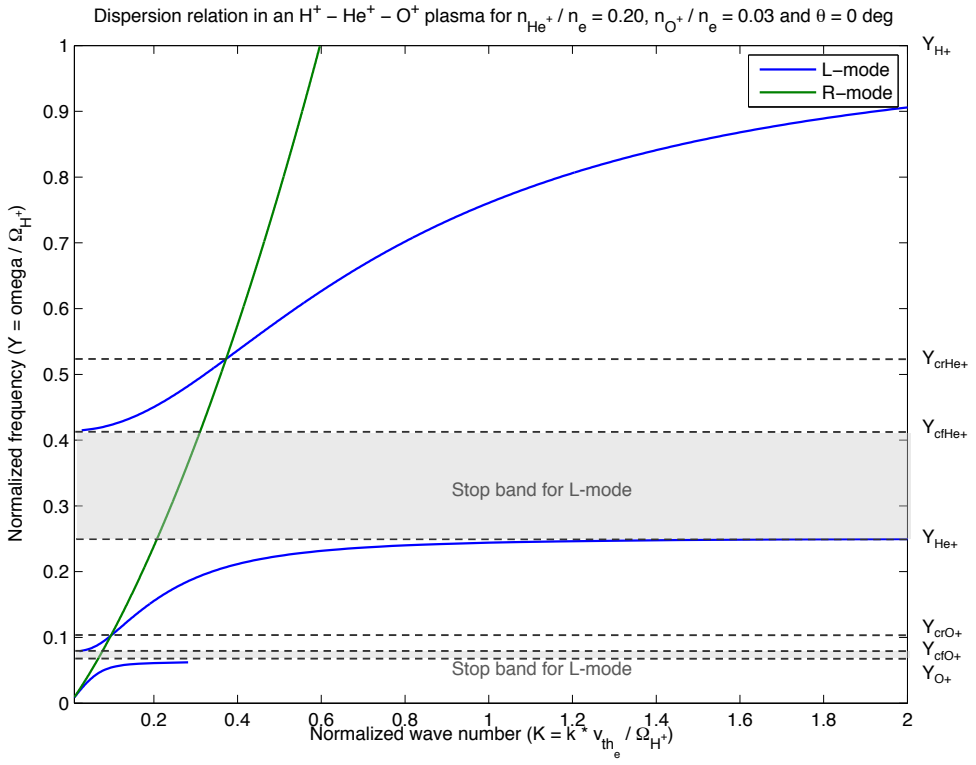

Figure 1.9: Dispersion relation for $\gamma_{H^+} = 0.77$, $\gamma_{He^+} = 0.20$, $\gamma_{O^+} = 0.03$ and $\theta = 0$.

1.2.5 Wave-Particle Interaction Processes

Consider a charged particle trapped in the belts. In the absence of waves, the particle performs an adiabatic motion. Neglecting the longitudinal drift, the relativistic equations of motion of the particle are given by

$$\dot{\vec{p}} = \frac{\vec{p}}{\gamma m} \times \vec{B}_0 \tag{1.34}$$

When we introduce an electromagnetic wave propagating obliquely with respect to the geomagnetic field, its effect adds to the adiabatic motion as follows

$$\dot{\vec{p}} = q\left[\vec{E}^w + \frac{\vec{p}}{\gamma m} \times \left(\vec{B}^w + \vec{B}_0\right)\right] \tag{1.35}$$

where q contains the charge of the particle and E_w and B_w are the electric and magnetic fields of the wave, respectively. The non-linear equations of motion for $(p_{II}, p_\perp, \eta)$ can be obtained from the

expression above, where η is the phase angle between the perpendicular component of the momentum and the left-hand component of the perpendicular magnetic field of the wave.

In order for the wave to introduce cumulative change of energy or momentum with the particle the wave vectors as seen by the particle must be stationary for a significant length of time, or in other words the Doppler shifted frequency as seen by the particle must equal its cyclotron frequency or a multiple of it

$$\omega - \vec{k}\cdot\vec{v} = l\frac{\Omega}{\gamma} \tag{1.36}$$

where ω is the wave frequency, Ω is the cyclotron frequency defined in Eq. 1.19, $\vec{k}$ is the wavenumber vector, $\vec{v}$ is the particle's velocity vector, γ is the relativistic factor and l is the harmonic number. This equation is the cyclotron resonance condition. Cyclotron interaction requires that protons move in the opposite direction to the L-mode waves ($l = 1$, EMIC), i.e. $\vec{k}\cdot\vec{v} < 0$, causing an upward shift in the frequency. On the other hand, electrons must overtake the wave to reverse the apparent sense of polarization to R-mode and with a velocity sufficient to Doppler shift the wave frequency to the relativistic electron gyrofrequency.

As an example, Figure 1.2.5 presents numerical and experimental results of the effect of man-made wave-particle interactions compared to other natural sources of scattering [1]. It can be observed that forced VLF emissions significantly reduce the precipitation lifetime of energetic particles (for $L < 3$).

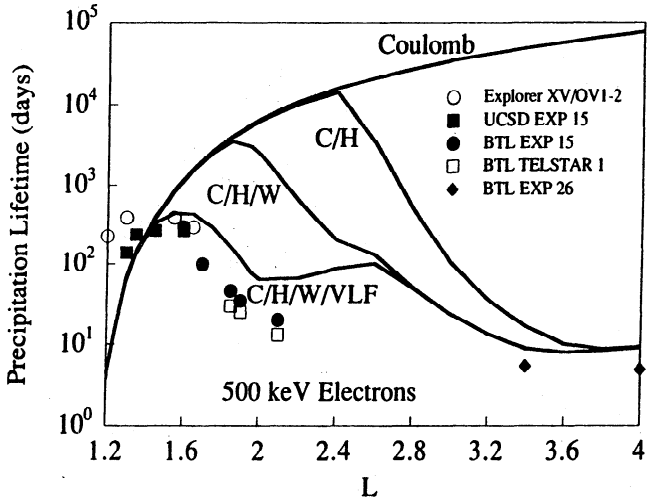

Figure 1.10: Precipitation lifetime for 500 keV electrons scattering due to Coulomb collisions (C), Coulomb and plasmaspheric hiss (C/H), Coulomb, plasmaspheric hiss and lightning-generated Whistlers (C/H/W), and with all scattering mechanisms included (C/H/W/VLF). [1]

1.3 Thesis Statement and Objectives

This study aims at characterizing the ability of Electromagnetic Ion Cyclotron (EMIC) waves to precipitate the energetic protons and electrons trapped in the Van Allen belts, and to translate these findings into engineering specifications of a spaceborne RBR system able to significantly reduce this energetic radiation. In order to fulfill this goal, the following objectives have been defined:

- Determine the type of antenna able to radiate EMIC waves in the magnetospheric plasma. This is a largely unexplored territory that should be addressed, given its potential practical importance.
- Characterize the radiation impedance and radiation pattern of this antenna in the far-field region.
- Study the cold plasma wave-propagation of the EMIC band radiated from the proposed antennae. In order to do that we will need to modify previously developed ray-tracing codes, which are able to handle Whistler waves.
- Characterize the interaction of the previous waves with the energetic population of particles in the belts. The waves are considered monochromatic and propagating at an angle to the geomagnetic field. Similar studies have been previously developed for Whistlers interacting with electrons, but no attention has been paid to the lower frequency and its interaction with both high-energy protons and electrons.
  - Study the scattering of a single particle. This analysis will determine the region in velocity space that includes all particles that can resonantly interact with the waves, which is an input to the distribution function.
  - Study the scattering of the magnetospheric energetic distribution using a test particle method.
- Characterize the feasibility in terms of power levels, frequencies, voltages, currents and mass of a potential spaceborne RBR antennae capable of significantly reduce the energetic radiation in the belts.
- Estimate precipitated fluxes and compare them with the values of typical background precipitation.

Chapter 2

Literature Review and Contributions

The main publications and findings relevant to my research are summarized next. They are classified into three groups, which correspond to the models being developed: radiation of ULF/VLF waves, their propagation and the study of wave-particle interactions. Existing engineering applications are discussed next, and the expected contributions from my thesis are summarized at the end of this section.

2.1 Radiation of ULF/VLF Waves

Prominent among the at least partially unsolved problems related to RBR is that of radiation of ULF/VLF waves from a space antenna, specially the non-linear effects occurring in the neighborhood of a kV transmitter in the presence of the background magnetized plasma. The impedance of an electric dipole transmitting in the VLF regime in a magnetoplasma has been determined in the absence of the plasma sheath [15, 118, 119, 120], and its current distribution has been analyzed under the same assumption [17, 28]. More specifically, the quasi-electrostatic approximation of Balmain [15] for the far-field is valid for any antenna orientation with respect to the Earth's magnetic field lines, and it basically neglects the electric field due to time variations of the perturbed magnetic field. Additional methods have been developed for the linear propagation part of the problem [31, 107]. In particular, we have in hand full-wave calculation methods for both Whistler and EMIC waves, and we have calibrated them by comparison to previous work [72, 120, 103] and to Balmain's approximation. One important conclusion is that Balmain's method has wider validity than generally recognized, because the radiation field is dominated by the near-resonance cone area, and this is precisely where the approximation is most accurate (whether or not the antenna is short). The Balmain approximation states that the

free-space wavenumber is small compared to the actual wavenumber, or equivalently, that the index of refraction is large. For many plasma waves like EMIC waves, resonances occur where the index of refraction approaches infinity for some special directions; it is in the vicinity of these directions that most of the radiation power propagates, thus the quasi-electrostatic approximation can be expected to have a wide range of validity [118]. However, for an electrical dipole antenna, the plasma involves the formation of a thick oscillatory sheath [27, 100, 112], the concentration of power around resonance cones, with potential for wave ducting [102], and the effects of this highly perturbed plasma region on the radiation impedance and on the self-consistent current distribution along the antenna.

The emission of the very low EMIC band entails additional complexity. The sheath around a space-based RBR antenna is very thick, and so its capacitance is almost the vacuum capacitance, which is nearly independent of the frequency and proportional to the transmitter length. If the frequency is in the Whistler band, the capacitive reactance is tolerable for antenna length of the order of 100 m or more. However, for the EMIC band, the associated reactance is extremely high even for a multi-km transmitter, to the point that it is not possible to use an electric dipole to radiate these waves without the help of any other device. On the other hand, in terms of the radiation resistance, a short antenna would be ideal, because the relevant wavelengths (those near the resonance cone) are indeed very short; unfortunately, short antennas suffer the most from the small capacitance problem, although even a multi-km antenna would have too much reactance at the EMIC regime. Non-capacitive antenna types, like loop antennae, need to be evaluated in this context, as well as electrostatic antennae that are capable of charge ejection to avoid accumulation during the oscillations. Except for linear far-field analyses of loop antennae [121, 117], the unrealized Soviet Active mission (Intercosmos 24) that failed to deploy a VLF loop antenna with the objective to understand its radiation properties and triggered particle precipitation [87], and DC bipolar plasma contactor experiments using reversible hollow cathodes [48], this is also a largely unexplored territory that should be addressed, given its potential practical importance.

2.2 Propagation of ULF/VLF Waves

The propagation of Whistler and EMIC waves has been studied through observations and ray-tracing simulations. Observations of EMIC waves from ground and space have been reported in different studies [10, 9, 33, 35, 36, 76] most frequently and most intense during geomagentic storms. The fact that they are observed on the ground indicate that they may mode-convert and tunnel through the bounce point [95]. In addition, ray-tracing codes have been developed to study the propagation of these waves and their correlation with observations. These codes use the eikonal approximation of geometrical optics [22] to follow the wave group velocity for given magnetic field and plasma density models. It has been shown [110] that the propagation vector tends to become oblique due to the

curvature of the Earth's magnetic field, but that the group velocity vector remains mostly aligned to the ambient field except in the vicinity of the bi-ion frequency, which is a mixed resonance between two ion species. At frequencies above the bi-ion frequency, EMIC waves exhibit a resonance cone that prevents them from getting perpendicular to the geomagnetic field, thus wave reflection cannot occur until they propagate to higher latitudes and the local bi-ion frequency increases above the wave frequency [109]. At the bi-ion frequency the wave-normal angle equals $\theta = 90°$, the parallel group velocity is zero and the wave is reflected [91], thus becoming trapped in the magnetosphere. This is analogous to the reflection of Whisters at the lower hybrid frequency [111]. This reflection and propagation is controlled by the concentration of heavy ions (especially He^+), which greatly influence the bi-ion frequency. Rauch and Roux [91] developed a three-dimensional ray tracing code for ULF waves propagating in an He^+-rich plasma; in the presence of this heavy ion, the dispersion relation of ULF waves splits into three branches [123]. Below each ion gyrofrequency the left-polarized mode propagates and is guided along the magnetic lines. For finite wave normal angles a crossover frequency exists between two cyclotron frequencies, where the polarization changes from left to right, while for field aligned waves both polarizations are decoupled. At 90° there is an additional resonance at the bi-ion frequency, which occurs between two cyclotron frequencies. Rauch and Roux showed that depending on the branch, left polarized waves can be guided along the field lines or unguided and compressional-like modes. Guided left-modes remain guided until the point where reflection occurs, where the wave frequency equals the local bi-ion hybrid frequency (and the wavenumber vector becomes perpendicular), but the wave may reach the ionosphere before this condition is met. Gomberoff and Neira [41] added a third cold ion species (O^+) and showed that it can affect the growth rate below the He^+ cyclotron frequency. Their publications considered waves propagating parallel to the magnetic field. Further studies [32, 77] added a finite perpendicular wavenumber, which means that Landau damping effects can take place due to the finite parallel electric field. Horne and Thorne [44] introduced the HOTRAY ray-tracing code to compute the propagation, growth and absorption of EMIC waves. More recently, complex studies have been presented that couple natural generation of EMIC, ray-tracing and wave-particle interactions [68, 70].

2.3 Wave-Particle Interaction

It has been observed that the precipitation of energetic particles from the Van Allen belts is strongly mediated by interactions with ULF/VLF waves. Evidence shows that naturally occurring Whistler band waves can precipitate energetic electrons [1, 24, 25, 58, 82] and EMIC waves can precipitate both energetic protons [33, 122] and electrons [75, 83, 84, 95]. There is evidence [49, 54, 71] that even the relatively small fraction of VLF power that leaks into the ionosphere from ground emission by a few high-power transmitters can have a strong-to-dominant effect on this precipitation, and hence on the

equilibrium population of trapped high-energy particles.

This has renewed interest in the wave-particle interaction between ULF/VLF waves and the high-energy particles of the radiation belts, which has been addressed by many authors in the past and keeps on being a hot topic. Three approaches have been used to study the problem. The main references and findings for each of these methods are summarized next.

One of the most common ways to deal with the problem consists of solving the pitch-angle diffusion equation for the distribution function of energetic particles, which involves the calculation of diffusion coefficients. Kennel and Petschek [65] showed that pitch-angle diffusion due to wave-particle interactions could be a dominant loss mechanism for energetic electrons, and Kennel and Engelmann [66] were the first to derive the general quasi-linear pitch-angle diffusion equation. Das [30] studied a wave pulse propagating through a plasma described by a Kennel and Petschek distribution function and Ashour-Abdalla [12] continued with the study of the effect of the modification of the distribution function on the Whister waves themselves using linear theory in the description of the particle's trajectories. Later, based on Kennel and Engelmann's formulation, Lyons et al. [80, 81, 78, 79] derived general expressions for the particle quasi-linear diffusion coefficients in both pitch angle and energy in an electron-proton medium valid for cyclotron resonance with any wave mode and distribution of wave energy, and particularized them to the interaction of Whisters and Ion Cyclotron waves with high-energy electrons and protons. Albert [3] introduced relativistic effects to the quasi-linear analysis of the interactions of either electrons or protons with either oblique Whister or ion cyclotron waves in an hydrogen plasma, and in a later publication [6] he studied the diffusion coefficients for oblique EMIC waves interacting with electrons in a multispecies plasma. Jordanova et al. [62, 63, 60, 61] introduced the effect of heavy ion species in the calculation of quasi-linear diffusion coefficients of incoherent EMIC waves interacting with protons. However, all these studies arbitrarily assigned wave polarization and spectral characteristics. Khazanov et al. addressed this issue in the development of a new self-consistent model of the interacting protons and electrons with naturally generated ion cyclotron waves; he first considered parallel propagation [69] and the effect of oblique waves was introduced in the following publications [68, 67]. Lotoaniu et al. [76] modeled the electron pitch-angle scattering due to the field-aligned EMIC waves observed by the CRRES spacecraft using multi-ion quasi-linear diffusion coefficients, and later, Li et al. [74] examined the pitch-angle scattering of electrons by field-aligned EMIC and hiss waves during the main and recovery phases of a storm. For the Whister regime, Abel and Thorne [1] calculated the precipitated fluxes and diffusion coefficients of energetic electrons due to natural phenomena and Whister emissions in a plasma with different ion species, and Horne and Thorne [45] introduced ray-tracing to the analysis. Inan et al. [54] used power scaling from Abel and Thorne's results to compare scattering of electrons due to Whister emissions from spaceborne versus ground transmitters. The more recent studies of Glauert and Horne [40] and Albert [7] developed relativistic computer codes that efficiently calculated the quasi-linear diffusion coefficients and solved

the interaction between oblique EMIC/Whister waves and electrons, and Summers [105] developed exact closed-form analytical expressions from classical quasi-linear diffusion theory for the diffusion coefficients for resonant interaction with field-aligned electromagnetic waves that can be evaluated using negligible CPU time.

Another way of approaching the problem consists of solving the non-linear equations of motion of the high-energy particles interacting with the waves. A test particle simulation is a widely used method to solve these equations. Compared to other approaches, this formulation allows one to deal with coherent and narrow-band waves, which are fundamentally different from those produced by incoherent signals. In the later case the particles perform a random walk in velocity space, whereas during the interaction with a coherent wave individual particles are not scattered randomly, but they stay in resonance long enough for the particle's pitch angle to be substantially changed through non-linear interactions. This method was initially proposed by Inan [50, 56], who described the gyroresonance interaction between coherent field-aligned Whister waves and energetic electrons in the case of continuous VLF wave interaction with the particle's distribution. This model was further extended to include the effect of temporal variation of the precipitated flux as a result of the interaction of short-duration VLF waves with electrons [23, 55], which was used in the calculation of the spatial distribution of electron precipitation caused by VLF signals from ground-based transmitters [57]. Chang and Inan [24, 26, 25] introduced relativistic effects to the formulation, and [51] used this approach to study gyroresonant pitch-angle scattering of energetic electrons by Whister waves for coherent versus incoherent waves, and the results were compared with those from the classical diffusion treatment. The gyroaveraged equations for obliquely propagating Whisters were initially introduced for the Laundau resonance by [59], and extended to higher order resonances by [16, 53, 93, ?, 108]. Recently, Bortnik et al. [20] introduced ray-tracing to study the linear interactions between precipitating radiation-belt electrons driven by lightning-generated Whisters, and Kulkarni et al. [73] incorporated ray-tracing [52] as well as Landau damping [18] effects to model the effect of space based VLF transmitters to the energetic electron precipitation. It must be mentioned that all these publications use the test particle approach to deal with Whister waves interacting with electrons, but no attention has been paid to the lower frequency band and its interaction with the high-energy particles.

The last approach to the problem uses a test particle simulation to solve the two-dimensional resonance-averaged Hamiltonian that describes the wave-particle interaction. Shklyar [99, 98] was the first to use this method to study the non-relativistic proton interaction with an oblique electrostatic VLF wave. He considered a strong inhomogeneity, which led to a random walk for the particle canonical momentum. Ginet and Heinemann [38] and Ginet and Albert [37] used this formulation to study the relativistic case of a test particle interacting with a small amplitude electromagnetic wave, but they did not include the passage through the resonance because the external magnetic field was assumed constant. This issue was addressed by Albert [2, 4, 5], who included the spatial dependence of the

resonance condition for a small monochromatic VLF wave interacting with relativistic test electrons. These publications showed that the type of behavior depends on the ratio (R) of the phase oscillation period at resonance to the time scale for passage through the resonance. For R>1 the interaction results in pitch angle and energy diffusion, but for R<1 phase bunching occurs, which translates to pitch-angle and energy change with well-defined signs and independent of the initial phase between the wave and the particle. In addition, Albert showed that phase trapping can occur when R<1 and that ratio is decreasing at resonance. For the EMIC band, Albert [8] used this formulation to study the non-linear interaction with relativistic electrons; however, interaction with energetic protons was not considered.

2.4 Engineering Applications

Many civil and military missions have tried to characterize the Van Allen belts and wave-particle interactions for years, but none has engineered and launched the RBR ideas yet. The Dynamics Explorer (DE) launched on 1981, Combined Release and Radiation Effects Satellite (CRRES) launched in 1990, Imager for Magnetopause-to-Aurora Global Exploration (IMAGE) launched on 2000 or the Radiation Belt Storm Probes (RBSP) to be launched on 2012 are examples of the first mentioned type. The only effort so far to test the Radiation Belt Remediation concept comes from the Air Force Research Laboratory (AFRL). AFRL's Demonstration and Science Experiments (DSX) is scheduled to be launched next October 2012 from Vandenberg Air Force Base, CA. The satellite features 14 payloads, grouped under three main experiments: the Wave Particle Interaction Experiment (WPIx), the Space Weather Experiment (SWx) and the Space Environmental Effects Experiment (SFx) [29, 101, 96, 39]. The WPIx entails a direct implementation of the Remediation ideas through the radiation of Whister waves from an 80 meter-long antenna and the characterization of their feasibility to reduce space radiation. One of the payloads required by this experiment is the Loss Cone Imager (LCI) [114], which is an electron loss-cone particle detector that will provide a 3D measurement of the energetic particle distributions. The High Sensitivity Telescope (HST) is a separate solid state detector telescope required in order to obtain fluxes of energetic electrons along the field lines. Where DSX is testing the efficacy of Whistler waves to alter the high-energy electrons in the radiation belts, the results of my thesis will serve to derive specifications for a potential RBR space-based system able to test the much lower EMIC band and its performance in precipitating not only the energetic electrons, but as well the even more harmful population of protons.

2.5 Thesis Contributions

My thesis aims at studying the radiation of coherent and narrow-band EMIC waves from a spaceborne transmitter, their propagation along the belts and their interaction with both high-energy protons and electrons. Numerous contributions arise from this study, which can be grouped in four groups:

- The radiation of this frequency band is a broad unexplored territory that should be addressed given its potential practical importance. In my thesis I will determine the type of antenna able to radiate EMIC waves in the magnetospheric plasma by addressing the solutions proposed above and determining their feasibility.

- Once the emitter's radiation pattern has been estimated, I plan to make use of the Stanford ray-tracing code to propagate the waves along the radiation belts, which would require adapting the implementation to my specific case.

- The interaction between these ray-paths and energetic particles will be analyzed next. In order to do that I am developing a test-particle simulation that solves the non-linear equations of motion. As mentioned above, this formulation is of especial interest to us because it allows one to deal with the non-linearities that may arise from interacting with coherent and narrow-band EMIC waves, as well as to easily introduce a short duration wave pulse (which would probably be the transmitter's operating mode). This analysis has two parts: (1) the study of a single sheet of particles in order to determine the region in velocity where they can resonantly interact with the waves and (2) the study of the scattering of the magnetospheric energetic distribution. These analyses have been previously developed for Whister waves resonating with electrons, but no attention has been paid to the lower frequency band and its interaction with high-energy particles.

- Finally, I will translate these results to engineering specifications of a space-based RBR system able of significantly reduce the concentration of energetic particles in the belts, and I will compare its performance with sources of natural precipitation. As mentioned above, the AFRL's Demonstration and Science Experiments (DSX) will deal with the whistler band and its interaction with electrons, but no system able to radiate EMIC waves and scatter protons has ever been proposed.

Chapter 3

Approach

3.1 Algorithm Overview

Four models constitute the simulation of the interaction between energetic particles and EMIC waves:

- Magnetospheric models
- Antenna radiation model
- Propagation model
- Wave-particle interaction model

The magnetospheric models of plasma density, composition and magnetic field are inputs to the rest of the code. The antenna radiation model generates inputs to the propagation model, which determines the characteristics of EMIC waves along the magnetic lines required for wave-particle interaction calculations. The magnetic lines are discretized in latitude, and for every time and latitude step the properties of the waves originated at the source antenna (radiation model) are updated using ray-tracing (propagation model). These properties are used to solve the non-linear equations of motion of test energetic particles from given distribution function interacting with the wave (wave-particle interaction model). The process is repeated for every time step and every latitude and the precipitated flux is calculated as a result of this iteration. This procedure is illustrated in Figure 3.1.

It must be noted that part of the complexity of this analysis resides in finding the right combination of antenna source location (antenna operations), wave characteristics (antenna design) and target particles (range of energies, pitch angles, etc.) that would provide the best result in terms of precipitation.

This iteration links with the translation to engineering specifications of a spaceborne system able to perform this mission.

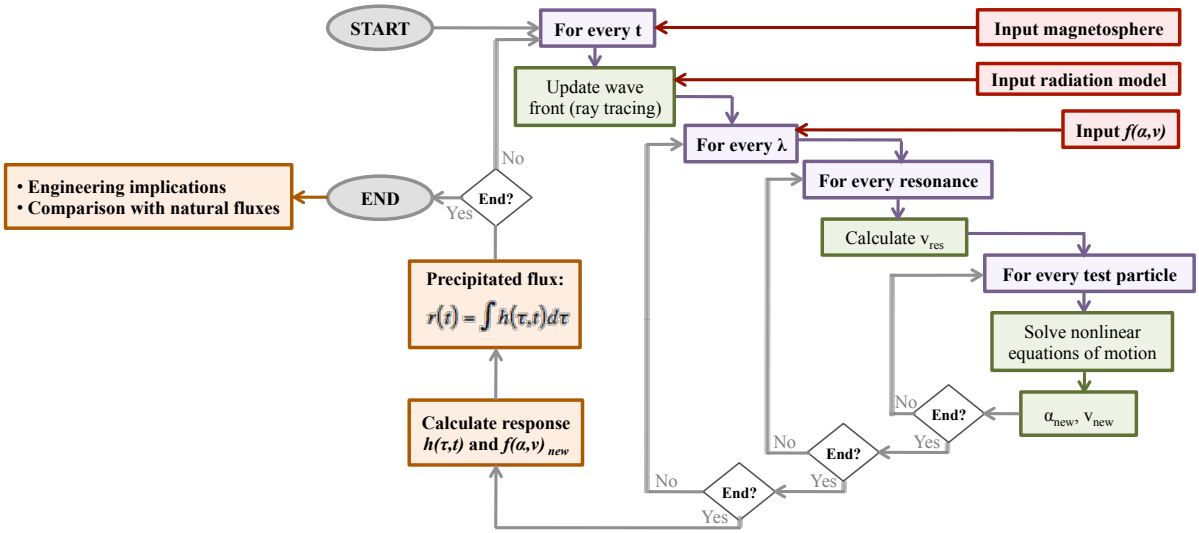

Figure 3.1: Algorithm schematic

3.2 Magnetospheric Models

Wave-particle interactions of interest to RBR happen within the inner mangetosphere, which covers the region up to $L = 6$ and between $\pm 66°$ of geomagnetic latitudes. Within this region, a dipole model represents a good approximation of the Earth's magnetic field, with dipole axis tilted with respect to the rotation axis by 11.5°. The strength of the magnetic field given by this model can be found as a function of the geocentric distance and the geomagnetic latitude as follows

$$B_0\,(r,\lambda) = B_0 \left(\frac{R_E}{r}\right)^3 \sqrt{1+3sin^2\lambda} \tag{3.1}$$

where r and λ are the geocentric radial distance and the geomagnetic latitude, respectively. $R_E = 6370\,km$ is the mean radius of the Earth and $B_0 = 3.12{\cdot}10^{-5}\,T$.

In the dipole model, the equation of a field line is given by

$$r\,cos^2\lambda_E = R_E cos^2\lambda \tag{3.2}$$

where λ_E is the latitude of the point where the field line intercepts the Earth's surface. The definition of the L-shell parameter comes from this equation, which identifies a given field line

$$L = \frac{r_{eq}}{R_E} = \frac{1}{cos^2\lambda_E} \tag{3.3}$$

In the inner magnetosphere, the background cold plasma can be represented using a diffusive equilibrium model [11]. Under these conditions, the variation of the electron density along the magnetic lines can be represented as follows

$$N_e\left(L,\, \lambda\right) = N_1\sqrt{\sum_j \xi_j e^{-z/H_j}} \tag{3.4}$$

where

$$z = r_1 - \frac{r_1^2}{r} - \frac{\omega_E}{2g_1}\left(r^2 cos^2\lambda - r_1^2 cos^2\lambda_1\right) \tag{3.5}$$

$$H_j = \frac{kT}{m_j g_1} \tag{3.6}$$

where ξ is the fraction of each ionic species, ω_E is the rate of rotation of the Earth, g is the gravity, k is the Boltzman's constant, T is the temperature and m is the particles mass. The subscript i refers to the different ionic species (H^+, He^+, O^+) and the subscript 1 to the reference level at 1000 km of altitude. Figure 3.2 [46] presents model and data densities and temperatures of different ion species at $L = 1.5 - 2.5$ as of November, 1981. The profiles correspond to the FLIP model while the markers refer to DE 1/2 data. For a given altitude, we observe that there is not much difference in the parameters from shell to shell.

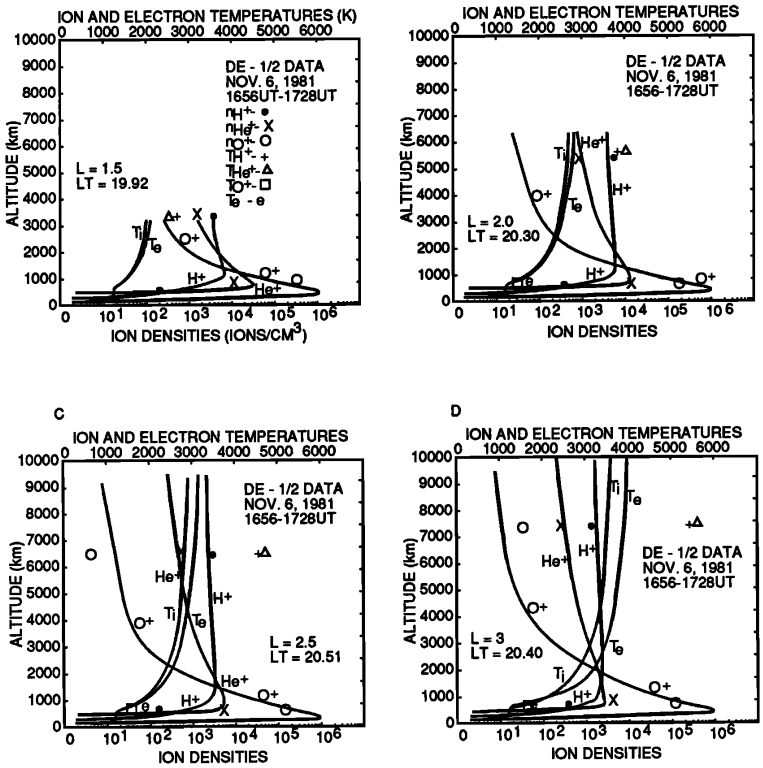

Figure 3.2: Altitudinal profile of ion densities and temperatures for L=1.5-2.5 [46]

3.3 The Radiation Model

This model aims at identifying a spaceborne antennae able to radiate waves in the EMIC band and to characterize its radiation impedance and radiation pattern.

The sheath around a space-based EMIC antenna is very thick, and so the antenna capacitance is almost the vacuum capacitance, which is very small and dominates. The associated reactance is extremely high for EMIC waves to the point that it is not possible to use an electric dipole to radiate these waves without the help of any other device. The radiation resistance of an electric dipole in a magnetoplasma perpendicular to the Earth's magnetic field is given by [15]

$$R_{rad} = \frac{2\,|p|}{\pi\omega\epsilon_0 S L_a}\left[Ln\left(\frac{L_a}{2r_a}\right) - 1 - Ln\left(\frac{\sqrt{1+p^2}}{2}\right)\right] \tag{3.7}$$

where L_a is the antenna length, r_a is its radius, $p^2 = S/P$ and P and S have been defined in Eqs. 1.15

and 1.16, respectively.

The antenna capacitance (slightly modified by the sheath) is given by [100]

$$X_{antenna} = \frac{1}{\pi\omega L_a \epsilon_0}\left[Ln\left(\frac{r_{sh}}{r_a} - \frac{1}{2}\right)\right] j \quad \Longrightarrow \quad C_{antenna} = \frac{1}{j\omega X_{antenna}} = \frac{\pi L_a \epsilon_0}{Ln\left(\frac{r_{sh}}{r_a} - \frac{1}{2}\right)} \tag{3.8}$$

which is mostly the vacuum capacitance

$$C_{vacuum} = \frac{\pi L_a \epsilon_0}{Ln\left(\frac{L_a}{2r_a}\right)} \tag{3.9}$$

where r_{sh} is the sheath's radius, which can be estimated using Song's formulation [100]. From these expressions we observe that a short antenna would be ideal in terms of radiation resistance, because the relevant wavelengths (those near the resonance cone) are indeed very short; unfortunately, short antennas suffer the most from the small capacitance problem, although even a multi-km antenna would have too much reactance at the EMIC regime.

In order to address this problem two possible solutions have been identified. The first option involves plasma contactors at both ends of a linear dipole, thus avoiding oscillatory charge accumulation responsible for the huge capacitive impedance. The second case under consideration consists of a magnetic loop dipole working as an EMIC transmitter. Wang and Bell [19, 116] calculated the radiation resistance of a small filamentary loop antenna in a cold magnetoplasma. Figure 3.3 shows this resistance versus the frequency normalized with the proton gyrofrequency. The two plots are for different normalized loop radius ($r_0 = \omega_{ce} r/c$) and for a plasma to electron cyclotron frequency of $\omega_{pe}/\omega_{ce} = 10$. To illustrate the difficulty of radiating EMIC waves with this antenna imagine that we require a radiation resistance of $R_{rad} = 10^{-5}\,\Omega$ in the EMIC range. According to this plot and assuming operation in $L = 2$ ($f_{ce} = 110\,kHz$), we would need a loop radius of $r = 218\,m$, which increases with increasing radiation resistance. If we aim at emitting 100 W of power, the input current to the antenna should be $I = 4.5\,kA$. This design implies a huge semiconductor magnetic loop dipole, which seems indeed not feasible.

Our future efforts in this area will focus on studying variations in the structure of a magnetic loop that could increase the radiation resistance with respect to that of a single loop, like multiple smaller loops or coil antennae.

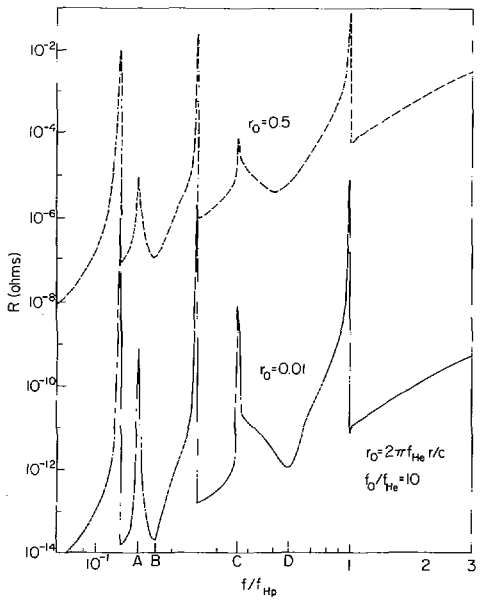

Figure 3.3: Loop radiation resistance as function of frequency in multi-ion plasma [19]

3.4 The Propagation Model

To describe the propagation of EMIC waves in the Earth's magnetosphere it is important to consider the variation of the geomagnetic field and the plasma density with location in space. Unlike the case of propagation in an homogeneous and isotropic medium where the wave-normal angle (phase velocity) lies in the direction of propagation of the wave energy (group velocity) , the magnetosphere is inhomogeneous and anisotropic and these two directions do not coincide in general. The trajectory of the wave energy is called ray path, and it is always perpendicular to the refracting index surface.

If the properties of the medium vary slowly within one wavelength we can use the geometric optics approximation to determine the entire trajectory of the ray path (wave energy). Geometric optics assumes that, within a given slab, the properties of the medium are locally constant and change slowly as the ray propagates to the next slab. This can be interpreted as successive applications of Snell's Law, i.e., $\mu_i cos\chi_i = \mu_{i+1} cos\chi_{i+1}$ as in Figure 3.4, where μ is the refractive index, and neglects partial reflections between slabs.

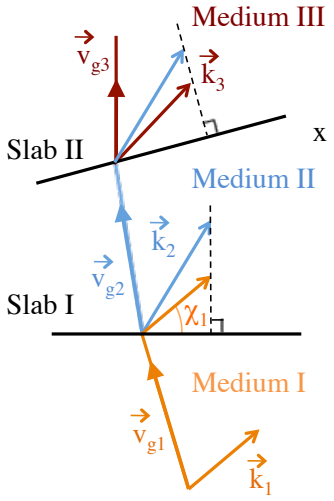

Figure 3.4: Snell's Law interpretation of ray tracing equations

The ray tracing equations were first derived by Haselgrove, 1955 [42] and they are a set of closed first order differential equations that can be integrated numerically. Although the original formulation was three dimensional, it is common to consider the 2D case and only trace rays in the meridional plane. The 2D differential equations are given by

$$\frac{dr}{dt} = \frac{1}{\mu^2}\left(\rho_r - \mu\frac{\partial\mu}{\partial\rho_r}\right) \tag{3.10}$$

$$\frac{d\varphi}{dt} = \frac{1}{r\mu^2}\left(\rho_\varphi - \mu\frac{\partial\mu}{\partial\rho_\varphi}\right) \tag{3.11}$$

$$\frac{d\rho_r}{dt} = \frac{1}{\mu}\frac{\partial\mu}{\partial r} + \rho_\varphi\frac{d\varphi}{dt} \tag{3.12}$$

$$\frac{d\rho_\varphi}{dt} = \frac{1}{r}\left(\frac{1}{\mu}\frac{\partial\mu}{\partial\varphi} - \rho_\varphi\frac{dr}{dt}\right) \tag{3.13}$$

where r and φ are the geocentric distance and colatitude respectively, ρ_r and ρ_φ are the radial and colatitude components of the refractive index vector (parallel to $\vec{k}$ with length μ) and t is the integration variable which has units of distance (t = phase time $\times$ speed of light). We must note here that the properties of the medium appear only through the refractive index μ and its components ρ_r and ρ_φ.

Given a set of initial values of ray position and wave-normal vector coming from the EMIC radiation

analysis, the integration of the ray tracing equations determines the variation of the these quantities as a function of distance.

3.5 The Wave-Particle Interaction Model

3.5.1 Non-linear Equations of Motion

Consider a test proton trapped in the belts under the influence of an EMIC wave with a wave vector $\vec{k}$ in the x-z plane, which is obliquely propagating with an angle ψ with respect to the -z axis. The Earth's magnetic field $\vec{B}_0$ is directed along the z-axis. The situation is represented in Figure 3.5. The wave fields can be written in the form

$$\vec{B}^w = B_x^w cos\Phi\, \hat{e}_x + B_y^w sin\Phi\, \hat{e}_y - B_z^w cos\Phi\, \hat{e}_z \tag{3.14}$$

$$\vec{E}^w = -E_x^w sin\Phi\, \hat{e}_x + E_y^w cos\Phi\, \hat{e}_y - E_z^w sin\Phi\, \hat{e}_z \tag{3.15}$$

where Φ is the wave phase defined as follows

$$\Phi = \int \omega dt - \int \vec{k}\cdot\vec{dr} \tag{3.16}$$

where ω is the wave frequency, $\vec{k}$ is the wavenumber vector and the integral is evaluated along the ray direction.

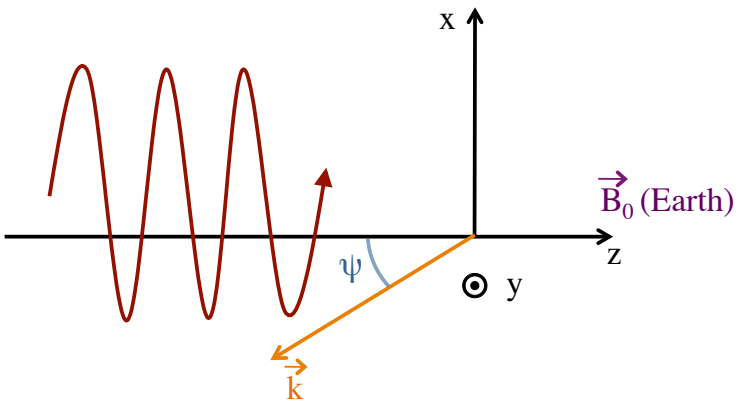

Figure 3.5: Schematic of the wave-particle interaction

The magnitude of the wave polarization ratios can be found from Maxwell's equations and are given by

$$\frac{E_x^w}{E_y^w} = \frac{S - n^2}{D} \tag{3.17}$$

$$\frac{E_z^w}{E_y^w} = \frac{\left(S - n^2\right) n^2 sin\theta cos\theta}{D\left(n^2 sin^2\theta - P\right)} \tag{3.18}$$

$$\frac{B_x^w}{B_y^w} = -\frac{D\left(n^2 sin^2\theta - P\right)}{P\left(S - n^2\right)} \tag{3.19}$$

$$\frac{B_z^w}{B_y^w} = -tan\theta \frac{D\left(n^2 sin^2\theta - P\right)}{P\left(S - n^2\right)} \tag{3.20}$$

where n is the refractive index defined in Eq. 1.26 and P, S and D have been defined in Eqs. 1.23 to 1.25.

The wave fields given above can be expressed as a sum of right and left circularly polarized components

$$\vec{B}^w = \vec{B}_R + \vec{B}_L - \vec{e}_z B_z^w cos\Phi \tag{3.21}$$

where

$$\vec{B}_R = \frac{B_x^w + B_y^w}{2}\left(\vec{e}_x cos\Phi + \vec{e}_y sin\Phi\right) \tag{3.22}$$

$$\vec{B}_L = \frac{B_x^w - B_y^w}{2}\left(\vec{e}_x cos\Phi - \vec{e}_y sin\Phi\right) \tag{3.23}$$

At a fixed point in space, $\vec{B}_R$ rotates counterclockwise about $\vec{B}_0$ with angular velocity ω, while $\vec{B}_L$ rotates clockwise.

The Earth's magnetic field is assumed to be locally parallel to the z-axis and vary slowly along it as follows

$$\vec{B}_0\left(\vec{r}\right) = \vec{B}_{0z}\left(z\right) + \vec{B}_{0\perp}\left(x, y, z\right) \tag{3.24}$$

where $\vec{B}_{0\perp}$ for a dipole model can be evaluated using a Taylor expansion in x and y

$$\vec{B}_{0\perp}(x,y,z) = -\left(\hat{e}_x cos\xi + \hat{e}_y sin\xi\right)\left(x\, cos\xi + y\,\hat{e}_y sin\xi\right)\frac{\partial B_{0z}}{\partial z} \tag{3.25}$$

where ξ is the angle between the magnetic meridional plane and the x-z plane.

We must mention here that all these equations including the dispersion relation in Section 1.2.4 are derived for an homogeneous medium. However, since the spatial variations of the plasma density and Earth's magnetic field are small over the distance of the order of the wavelength, at any given point we can assume that the wave has the same characteristics as those of a wave traveling in an homogeneous medium with the same refractive index. This constitutes the slowly varying approximation, which is commonly known as WKB approximation.

According to the resonance condition given in Eq. 1.36, protons must travel in the opposite direction to the waves, causing an upward Doppler shift on the frequency. Substituting these expressions into the Lorentz force equation (Eq. 1.35) we get the following scalar equations of motion of the traveling particle

$$\dot{p}_x = -qE_x^w sin\Phi + \frac{q}{m_p\gamma}\left[p_y\left(-B_z^w cos\Phi + B_{0z}\right) - p_z\left(B_y^w sin\Phi + B_{0\perp y}\right)\right] \tag{3.26}$$

$$\dot{p}_y = qE_y^w cos\Phi + \frac{q}{m_p\gamma}\left[-p_x\left(-B_z^w cos\Phi + B_{0z}\right) + p_z\left(B_x^w cos\Phi + B_{0\perp x}\right)\right] \tag{3.27}$$

$$\dot{p}_z = -qE_z^w sin\Phi + \frac{q}{m_p\gamma}\left[p_x\left(B_y^w sin\Phi + B_{0\perp y}\right) - p_y\left(B_x^w cos\Phi + B_{0\perp x}\right)\right] \tag{3.28}$$

which can be expressed in terms of parallel and perpendicular momentum to the Earth's magnetic field. Since the resonant interaction between a test proton and EMIC waves happens when the particle gyration is in phase with the left-hand elliptically polarized component of the wave, the angle in between $\vec{B}_L$ and $\vec{p}_\perp$ (φ) is the most appropriate third component to use in the derivation of the equations of motion. This angle is represented in Figure 3.6.

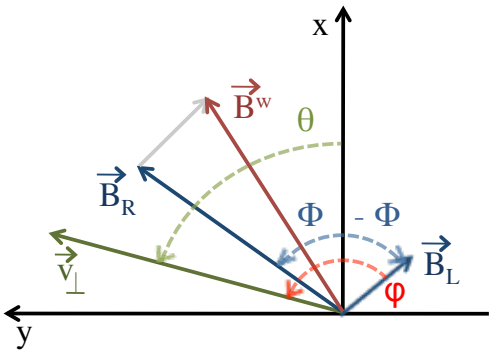

Figure 3.6: Phase geometry of the interaction process

Taking into account that

$$p_x = p_\perp cos\theta \tag{3.29}$$

$$p_y = p_\perp sin\theta \tag{3.30}$$

$$\theta = \varphi - \Phi \tag{3.31}$$

$$\dot{\Phi} = \omega - \vec{v}\cdot\vec{k} = \omega + v_x k_x + v_z k_z \tag{3.32}$$

the scalar equations of motion can be expressed as follows

$$\dot{\varphi} = \dot{\theta} + \dot{\Phi} = -\frac{\omega_{cp}}{\gamma} + \omega + v_x k_x + v_z k_z + \frac{C_1}{\gamma} \tag{3.33}$$

$$\dot{p}_z = -qE_z^w sin\Phi - \frac{1}{\gamma}\omega_1 p_\perp sin\left(\varphi - 2\Phi\right) - \frac{1}{\gamma}\omega_2 p_\perp sin\varphi + C_2 \tag{3.34}$$

$$\dot{p}_\perp = \omega_1\left(\frac{p_z}{\gamma} + R_1 m_p\right) sin\left(\varphi - 2\Phi\right) + \omega_2\left(\frac{p_z}{\gamma} - R_2 m_p\right) sin\varphi + C_3 \tag{3.35}$$

where m_p and ω_{cp} are the mass and cyclotron frequency of protons and

$$\omega_1 = \frac{q}{m_p}\frac{B_x^w + B_y^w}{2} \quad , \quad \omega_2 = \frac{q}{m_p}\frac{B_x^w - B_y^w}{2} \tag{3.36}$$

$$R_1 = \frac{E_x^w + E_y^w}{B_x^w + B_y^w} \quad , \quad R_2 = \frac{E_x^w - E_y^w}{B_x^w - B_y^w} \tag{3.37}$$

$$C_1 = \frac{q}{m_p}\frac{p_z}{p_\perp}\left[B_{0\perp x} cos\left(\varphi - \Phi\right) + B_{0\perp y} sin\left(\varphi - \Phi\right)\right] \tag{3.38}$$

$$C_2 = \frac{q}{m_p \gamma} p_\perp \left[B_{0\perp y} cos\left(\varphi - \Phi\right) - B_{0\perp x} sin\left(\varphi - \Phi\right)\right] \tag{3.39}$$

$$C_3 = \frac{q}{m_p \gamma} p_z \left[B_{0\perp x} sin\left(\varphi - \Phi\right) - B_{0\perp y} cos\left(\varphi - \Phi\right)\right] \tag{3.40}$$

In must be noted that in the equation for $\dot{\varphi}$ only the first order terms have been kept (we have neglected the effect of the wave-field on the equation for $\dot{\varphi}$). These equations can be simplified by taking the average over the particle gyroperiod. This approximation can be done if the gyroperiod of the proton is short compared to the time scale of the wave particle interaction. This approximation seems very reasonable and will be checked when solving the wave-particle interaction problem numerically. Following Jasna's formulation [92], we introduce three new variables

$$\chi = \int k_x dx \quad \Rightarrow \quad \dot{\chi} = k_x v_x \tag{3.41}$$

$$\varphi = \eta + \chi \quad \Rightarrow \quad \dot{\varphi} = \dot{\eta} + \dot{\chi} \tag{3.42}$$

$$\dot{\varphi} = -\frac{\omega_{cp}}{\gamma} + \omega + v_x k_x + v_z k_z \quad \Rightarrow \quad \varphi = -\frac{\omega_{cp}}{\gamma} t + \Phi + \Phi_0 - \varphi_0 \tag{3.43}$$

$$\Phi = \frac{\omega_{cp}}{\gamma} t + \theta_0 + \varphi = \sigma + \varphi = \sigma + \eta + \chi \tag{3.44}$$

$$\sigma = \frac{\omega_{cp}}{\gamma} t + \theta_0 \ , \quad \theta_0 = \varphi_0 - \Phi_0 \tag{3.45}$$

and substituting into Eqs. 3.33 to 3.35, we can rewrite the equations of motion as follows

$$\dot{\eta} = -\frac{\omega_{cp}}{\gamma} + \omega + v_z k_z + \frac{C_1}{\gamma} \tag{3.46}$$

$$\dot{p}_z = \omega_{\tau 0}^2 \frac{1}{k_z} \left[-\alpha_1 sin\left(\eta + \chi\right) - \gamma \alpha_2 sin\left(\sigma + \eta + \chi\right) + sin\left(2\sigma + \eta + \chi\right) \right] + C_2 \tag{3.47}$$

$$\dot{p}_\perp = -\omega_1 \left(\frac{p_z}{\gamma} + R_1 m_p \right) sin\left(2\sigma + \eta + \chi\right) + \omega_2 \left(\frac{p_z}{\gamma} - R_2 m_p \right) sin\left(\eta + \chi\right) + C_3 \tag{3.48}$$

where

$$\omega_{\tau 0}^2 = \frac{\omega_1 k_z p_\perp}{\gamma} \quad , \quad \alpha_1 = \frac{\omega_2}{\omega_1} \quad , \quad \alpha_2 = \frac{q E_z^w}{\omega_1 p_\perp} \tag{3.49}$$

Using the fact that

$$\chi = \int k_x dx = k_x v_\perp \int cos\left(\varphi - \Phi\right) dt = k_x v_\perp \int cos\left(\sigma\right) dt = \beta \, sin\sigma \tag{3.50}$$

where $\beta = \gamma k_x v_\perp / \omega_c$, and taking into account that

$$e^{i\beta sin\sigma} = \sum_{m=-\infty}^{m=\infty} J_m\left(\beta\right) e^{im\sigma} \tag{3.51}$$

the gyroaveraged equations of motion can be written as follows

$$\dot{\eta} = -\frac{\omega_{cp}}{\gamma} + \omega + v_z k_z + \frac{\underline{C_1}}{\gamma} \tag{3.52}$$

$$\dot{p}_z = \omega_{\tau 0}^2 \frac{1}{k_z} \left[-\alpha_1 J_0\left(\beta\right) + \gamma \alpha_2 J_1\left(\beta\right) + J_2\left(\beta\right) \right] sin\eta + \underline{C_2} \tag{3.53}$$

$$\dot{p}_\perp = \left[-\omega_1 \left(\frac{p_z}{\gamma} + R_1 m_p \right) J_2\left(\beta\right) + \omega_2 \left(\frac{p_z}{\gamma} - R_2 m_p \right) J_0\left(\beta\right) \right] sin\eta + \underline{C_3} \tag{3.54}$$

where $J_\nu\left(\beta\right)$ are the Bessel functions of order ν and argument β and

$$\underline{C_1} = 0 \tag{3.55}$$

$$\underline{C_2} = -\frac{1}{\gamma m_p}\frac{p_\perp^2}{2\omega_c}\frac{\partial \omega_c}{\partial z} \tag{3.56}$$

$$\underline{C_3} = \frac{1}{\gamma m_p}\frac{p_\perp p_z}{2\omega_c}\frac{\partial \omega_c}{\partial z} \tag{3.57}$$

From these equations we can see that the usefulness of η arises from the fact that $\eta \approx \underline{\eta}$ and it can be interpreted as the value of φ averaged over one gyroperiod.

3.5.2 Interaction with Individual Test Particles

When integrated over time, the equations of motion derived above determine the velocity space trajectories of individual test particles. This is the starting point of our study, which concerns the interaction between single particles and EMIC waves.

Previous studies of interaction between Whistlers and electrons [50] showed that the scattering is strongly dependent on initial Larmor phase, thus we expect a similar behavior for EMIC-proton interaction. For this reason, we will study protons at the edge of the loss cone, with different energies and distributed uniformly over initial phase.

In order to find the total scattering, the field line is discretized in latitude and the equations of motion are integrated along that path. This procedure is repeated for each test particle. Using the adiabatic motion relations, the integrated pitch angle and parallel velocity at each point along the path can be referred to the equator and compared to the initial equatorial values in order to find the total scattering and energy change of the particle.

The main result of this study is the region in velocity and pitch angle space that includes all particles that can resonantly interact with the radiated waves and that could be scattered into the loss cone. This information will be used as an input to the analysis of the full distribution of particles detailed in the next section.

3.5.3 Interaction with a Full Distribution of Particles

The test particles' study illustrates the dynamics of the interaction and provides information about the velocity and pitch angle space that includes all resonant particles. However, the analysis of the full distribution is required to assess the effects of EMIC waves on the population of energetic particles in terms of precipitated fluxes and lifetimes.

The trapped population of energetic particles along a geomagnetic field line can be represented by a distribution function at the equator $f(E,\alpha)$ in $part/\left[(m/s)^3\, m^3\right]$. However, experimental data are

often given in terms of the differential energy flux spectrum Φ_E in $part/\left(m^2 s\, sr\, J\right)$. We can relate these two quantities using conservation of particles as follows

$$\Phi_E\left(E,\alpha\right) dA\, d\Omega\, dE\, dt = f\left(E,\alpha\right) v^2\, dv\, d\Omega\, v dt\, dA \tag{3.58}$$

where $d\Omega$ is the element of solid angle and v is the magnitude of the velocity of a particle with energy E. Noting that $dE = m\gamma_E^3 v\, dv$, where γ_E is the relativistic factor associated with E, we find the following relation

$$f\left(E,\alpha\right) = \Phi_E\left(E,\alpha\right) \frac{m\gamma_E^3}{v^2} \tag{3.59}$$

The differential precipitated flux Φ in $part/\left(m^2 s\, J\right)$ can be obtained by integrating the wave-perturbed Φ_E over the solid angle representing the loss cone, which is given by $d\Omega = sin\alpha\, d\alpha\, d\phi$. The parallel flux includes $cos\alpha$ to project along the $\vec{B}_0$ tube. In addition, the result needs to be multiplied by B_{TP}/B_{eq}, which accounts for the reduction of the flux tube cross section; using Eq. 3.1 it can be shown that $B_{TP}/B_{eq} = \sqrt{1+3sin^2\lambda_{TP}}/cos^6\lambda_{TP}$, where λ_{TP} is the latitude at 100 km. The integral can be expressed as follows

$$\Phi\left(E\right) = 2\pi \frac{\sqrt{1+3sin^2\lambda_{TP}}}{cos^6\lambda_{TP}} \int_0^{\alpha_{lc}} \Phi_E\left(E,\alpha\right) cos\alpha\, sin\alpha\, d\alpha \tag{3.60}$$

and the number flux of precipitated particles N in $part/\left(m^2 s\right)$ would be

$$N = \int_E \Phi\left(E\right) dE \tag{3.61}$$

and the associated energy flux Q in $J/\left(m^2 s\right)$

$$Q = \int_E E\, \Phi\left(E\right) dE \tag{3.62}$$

We must note that by changing the limits of integration of N and Q we can explore the energy dependence of these two quantities. In addition, for the case of a traveling pulse (instead of a steady state case), all these quantities would be dependent on the time after pulse transmission.

The full distribution is simulated by a large number of individual test particles. For the high-energy population trapped in every flux tube, the distribution can be specified with its equatorial value $f_{eq}\left(v_{II0eq}, \alpha_{0eq}\right)$. From now on, we will drop the subscript eq. For a given field line and wave, only a portion of the total population is scattered by the wave. Therefore, we only need to consider that

portion of the distribution. These bounds are the result of the analysis of individual test particle trajectories. After the non-perturbed distribution is specified, each test particle is allowed to go through a complete interaction by solving the non-linear equations of motion between two points along a given field line. At the end of the interaction, each test particle would have acquired a new parallel velocity and pitch-angle, which can be identified with a mesh point (v_{IIF}, α_F) at the equator. This means that all the particles represented by this test particle have acquired parallel velocities and pitch angles between $v_{IIF} \pm (\Delta v_{II}/2)$ and $\alpha_F \pm (\Delta\alpha/2)$. Finally, in order to conserve the total number density of particles in the system, the distribution function at (v_{II0}, α_0) and at (v_{IIF}, α_F) needs to be modified as follows

$$f_{new}\left(v_{II0}, \alpha_0\right) = f_{old}\left(v_{II0}, \alpha_0\right) - \frac{1}{n_\phi} f_{old}\left(v_{II0}, \alpha_0\right) \tag{3.63}$$

$$f_{new}\left(v_{IIF}, \alpha_F\right) = f_{old}\left(v_{IIF}, \alpha_F\right) + \frac{1}{n_\phi} f_{old}\left(v_{II0}, \alpha_0\right) \frac{v_{II0}^2 \frac{sin\alpha_0}{cos^3\alpha_0}}{v_{IIF}^2 \frac{sin\alpha_F}{cos^3\alpha_F}} \tag{3.64}$$

where n_ϕ is the number of particles per cell uniformly distributed in phase angle. The perturbed distribution is obtained by using n_ϕ test particles per mesh point and repeating the procedure for every mesh point.

Chapter 4

Results to Date

Together with the formulation and conclusions presented in Chapters 1 and 3, my work to date consisted of the development of a wave-particle interaction code. My strategy starts by reproducing previous work of whistlers interacting with electrons, which allows one to validate the approach and methodology. Once the different aspects of this interaction have been checked with previous publications I can safely start changing the wave dispersion, propagation and target particles to address our problem. So far I have reproduced most of the work relative to whistlers (without ray-tracing of the waves) interacting with electrons using a formulation based on non-linear equations of motion, an I have started introducing the new EMIC regime and proton interaction. Some of the results obtained so far are presented next.

4.1 Whistlers and Electrons

My first step was to reproduce the very first test particle formulation from Inan, 1978 [56]. In his work, Inan studied the non-linear, non-relativistic cyclotron resonant interaction between electrons with coherent and ducted Whistler waves in steady state. He developed a test particle simulation to solve the non-linear equations of motion and calculated the precipitated energy fluxes due to the interaction with a full distribution of energetic particles. My first implementation reproduced these results, which are represented in Figures 4.1 and 4.2. The first plot gives the final net scattering at $L = 4$ ($n_{eq} = 400\, el/cm^3$) of a single resonant sheet of electrons uniformly distributed in Larmor phase ϕ, with an initial equatorial pitch angle of $\alpha_{eq0} = 10^\circ$ and moving away from the equator. The wave is characterized by $B_{w_{eq}} = 20\, pT$ and $f = 5\, kHz$, and the velocity of the particles is such that the interaction starts at the equator, which allows to clearly present the initial phase dependence. The

results are obtained by integrating the full equations of motions for each of the test electrons. In this picture we can observe that the interaction is non-linear and the scattering is larger at $\phi_0 \approx 0°$ due to a trapping process that occurs at preferential phases where most of the cumulative interaction takes place (phase trapping). Non-linear effects appear when the wave forces are the dominant factor in controlling the phase rather than the inhomogeneity of the geomagnetic field, which begins to happen for wave amplitudes greater than $B_{w_{eq}} = 3\,pT$.

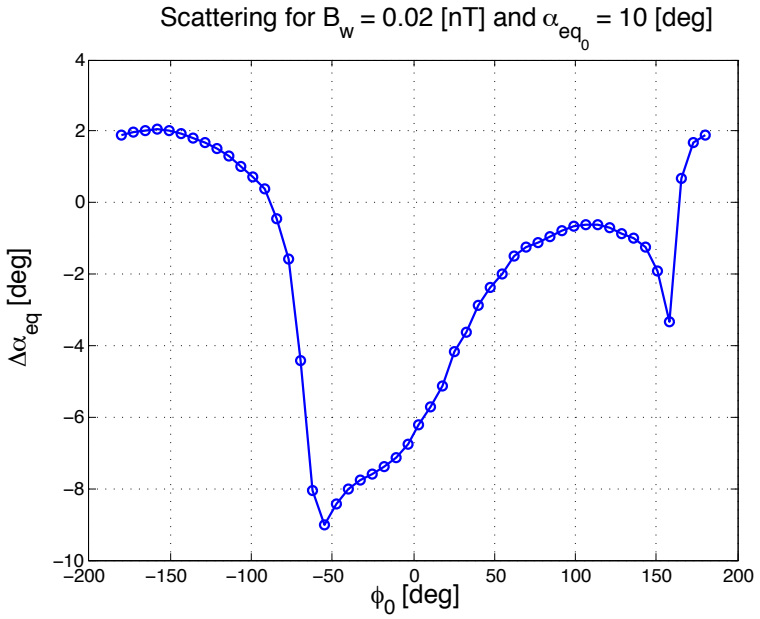

Figure 4.1: Total scattering versus initial phase for equatorially resonant electrons with $\alpha_{eq0} = 10°$, wave intensity of $B_w = 20\,pT$ and $f = 5\,kHz$

Figure 4.2 shows the equatorial distribution of particles integrated over parallel velocities between 1 to 2 keV. The distribution before (blue) and after (red) the interaction with a $B_{w_{eq}} = 30\,pT$ wave is presented. Particles are considered to be precipitated if their equatorial pitch angle after the interaction is smaller than the equatorial loss cone angle. Only the part of the distribution able to interact with this wave has been considered, which is uniform in pitch angle and has a sharp cutoff at the loss cone. We observe that as a result of the interaction, particles have been scattered into the loss cone. The energy flux of precipitated particles can be calculated according to Section 3.5.3, which gives $Q = 0.2\,J/\left(m^2 s\right)$ for $B_{w_{eq}} = 30\,pT$, in accordance with Inan's results.

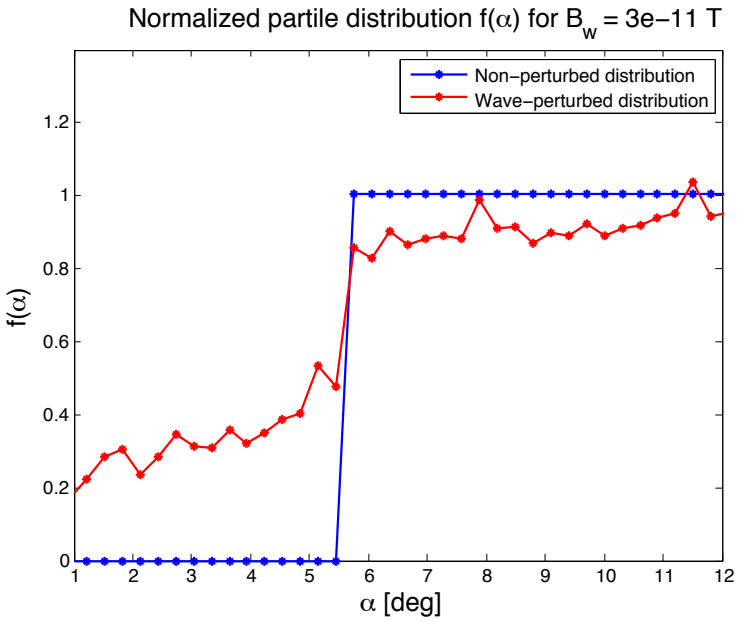

Figure 4.2: Non-perturbed and perturbed particle distribution versus equatorial pitch angle for $B_w = 30\,pT$ and $f = 5\,kHz$

The next step in the implementation was to include the temporal variation of the precipitated flux as a result of the interaction of short-duration Whistler pulses with energetic electrons [55] instead of considering steady state. Figure 4.3 shows the precipitated energy flux versus time after transmission of the wave injected at 1000 km of altitude at $L = 4$ for $B_{w_{eq}} = 5\,pT$ at the equator and $f = 6.83\,kHz$. The responses were calculated for pulse-front locations between $-16°$ and $44°$ of latitude. It can be observed that the total length of the precipitated pulse is about 4 seconds, and the flux peaks at 3.5 seconds. This maximum is the result of a convergence effect due to the responses' overlap at different pulse locations (thus different energies of interacting particles and different interaction lengths). Figure 4.4 shows the energy of the particles that corresponds to that flux versus time after transmission (each segment represents a step in the pulse location).

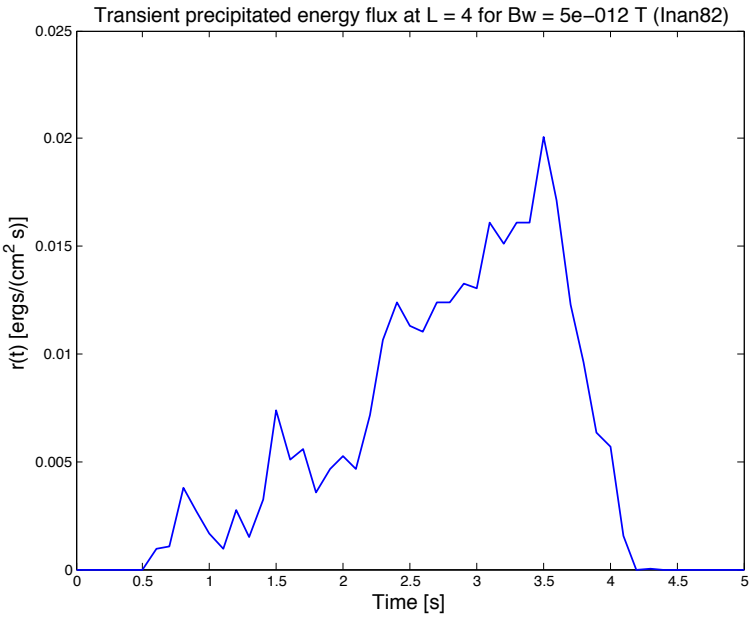

Figure 4.3: Precipitated energy flux versus time after the injection of the wave for $B_w = 5\,pT$ and $f = 6.83\,kHz$

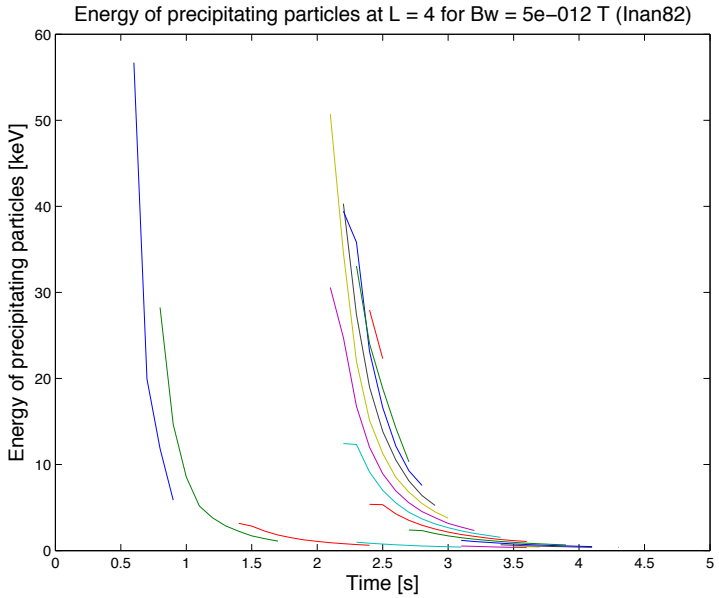

Figure 4.4: Energy of the particles that constitue the flux of Figure 4.3

The next analysis incorporated relativistic effects to the previous formulation. This work was developed in the past by Chang, 1983 [24] for the steady state case. The same author addressed the transient case in 1985 [26]. It must be noted here that relativistic effects are important when dealing with the energetic population of electrons trapped in the belts. However, these corrections would not be required when targeting energetic protons because their energy can be larger than the ones of electrons but their velocities are non-relativistic. Figure 4.5 presents the energy spectrum of near-loss-cone quasi-relativistic electrons for the steady state case at $L = 2$ ($n_{eq} = 800\, el/cm^3$), for a wave intensity of $B_{w_{eq}} = 7.5\, pT$ and $f = 5.46\, kHz$. The interaction takes into account two single passes, one at each side of the equator, and the number of lobes and width depends of the distance between these resonances.

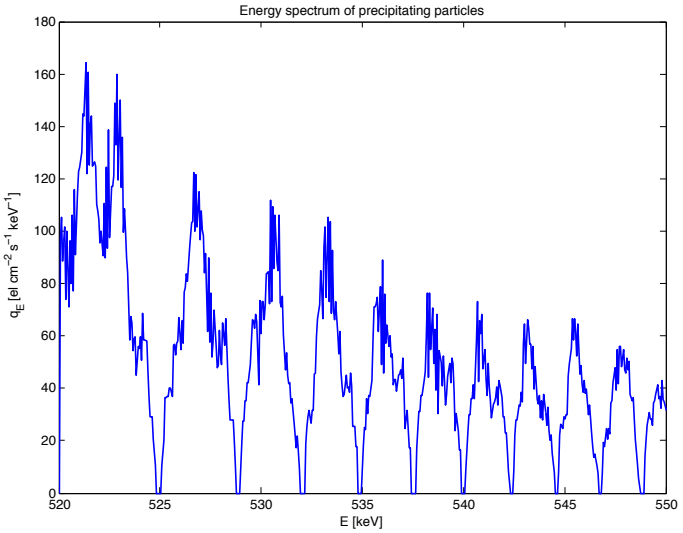

Figure 4.5: Energy spectrum of precipitating particles

Figures 4.6 to 4.8 reproduce Chang's results for relativistic electrons interacting with a 0.5 seconds Whistler pulse which enters the magnetosphere at 1000 km of altitude and propagates along $L = 4$ ($n_{eq} = 400\, el/cm^3$). The wave magnetic field intensity and frequency at the equator are taken to be $B_{w_{eq}} = 5\, pT$ and $f = 2.5\, kHz$. As the input pulse propagates toward the equator, it first interacts with higher energy electrons because the resonant electron energy decreases when approaching the equator (as indicated by the resonance condition in Eq. 1.28). These electrons arrive first to the precipitation region near the wave injection point, and equatorial scattered particles arrive later. As the pulse travels past the equator, it interacts again with higher energy electrons and, although interacting with the wave at later times, they can overtake these electrons scattered earlier by the wave close to the equator. This explanation matches the results presented in Figure 4.6, where the dynamic spectra of the precipitated energy flux is presented versus the particles' energy and the time after transmission.

Figures 4.7 and 4.8 present the integration of this spectra over energy and time, respectively.

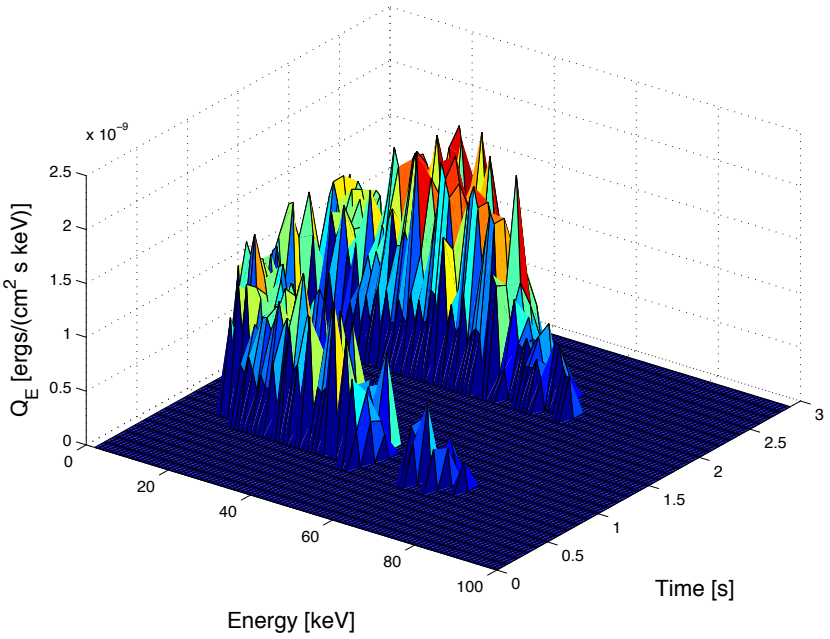

Figure 4.6: Dynamic spectra of the wave induced flux for $B_w = 5\,pT$ and $E_0 = 100\,keV$

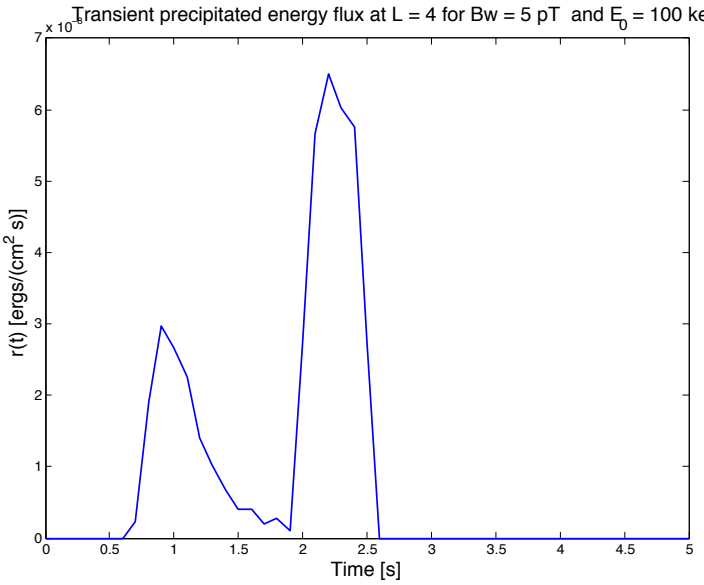

Figure 4.7: Transient precipitated energy flux for $B_w = 5\,pT$ and $E_0 = 100\,keV$

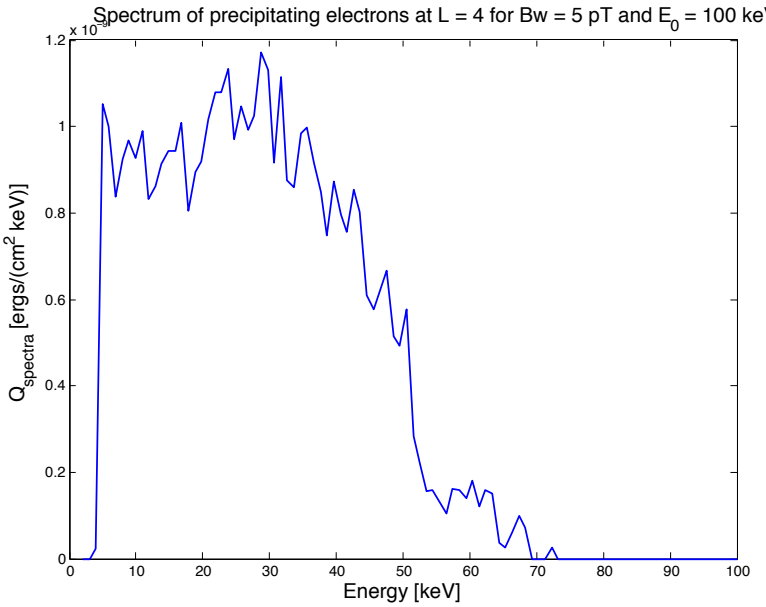

Figure 4.8: Spectrum of precipitating electrons for $B_w = 5\,pT$ and $E_0 = 100\,keV$

The effect of obliquely propagating Whistlers on electrons was introduced next. Figures 4.9 to 4.11 reproduce the work by Ristic [92, ?], which modeled the interaction between Whistlers propagating at a wave-normal angle of $\psi = 60°$, $f = 15.792\,kHz$ and constant power flux of $S = 8.1\,pW/m^2$ and electrons with energies around 100 eV at $L = 3$. Figure 4.9 presents the scattering (upper plot) and parallel velocity change (lower plot) of a single sheet of particles as a function of latitude due to that wave. The sheet corresponds to test electrons with the same initial velocity and pitch angle, and uniformly distributed in Larmor phase (each line corresponds to a different phase). We can observe that the scattering is strongly dependent on initial phase, and for the given parameters the rms scattering of the sheet has a value of $\Delta\alpha_{eq}|_{rms} = 1.04°$. For the same wave parameters, Figure 4.10 presents the perturbed distribution function referred to the equator after the interaction with the wave; we can observe that some particles have precipitated inside the loss cone, which is located at $\alpha_{lc_{eq}} = 8.62°$. Finally, Figure 4.11 presents the differential precipitated flux $\Phi(E)$ for the same case. The number flux of precipitated particles can be found by integrating $\Phi(E)$ over energies around 100 eV; taking $\Delta E = 0.2\,eV$, we get $N = 35{\cdot}10^4\,el/\left(cm^2 s\right)$.

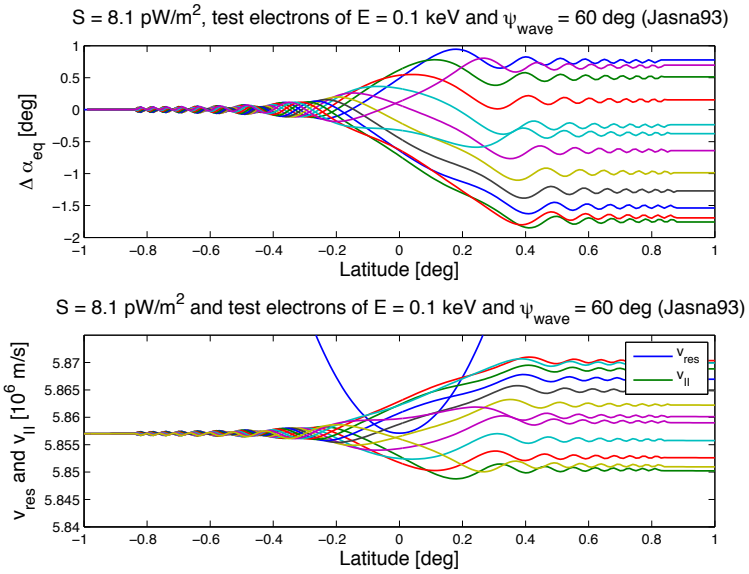

Figure 4.9: Scattering and parallel velocity of a sheet of electrons interacting with Whistlers with $\psi = 60°$, $f = 15.792\,kHz$ and $S = 8.1\,pW/m^2$ at $L = 3$

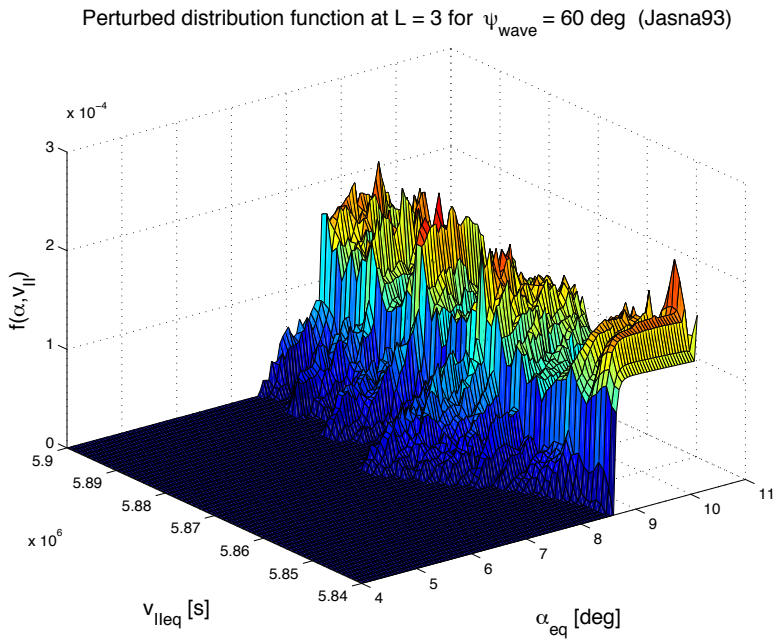

Figure 4.10: Perturbed distribution function due to a $\psi = 60°$, $f = 15.792\,kHz$ and $S = 8.1\,pW/m^2$ Whistler wave at $L = 3$

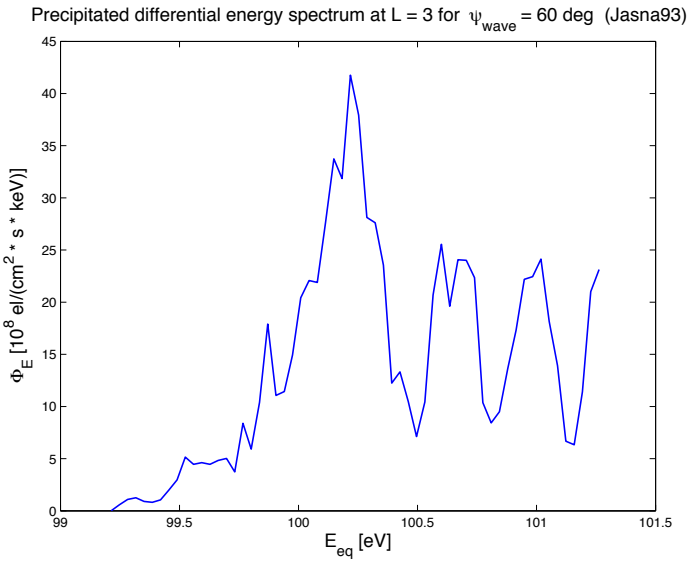

Figure 4.11: Differential precipitated flux of electrons due to a $\psi = 60°$, $f = 15.792\,kHz$ and $S = 8.1\,pW/m^2$ Whistler wave at $L = 3$

4.2 EMIC and Protons

The analyses above relative to whistler-electron interaction allowed me to validate the methodology being developed. Although the whistler-electron picture is still not complete, I have most of the ingredients to start analyzing the case of EMIC-protons. Next, I present my first steps in this direction, which address the implementation of the dispersion relation presented in Section 1.2.4 and the analysis of the resonance condition of protons and the EMIC wave band. This is an ongoing study that will result in the compatible range of frequencies, particles' energies and shells of operation input to the wave-particle interaction analysis. Figure 4.12 presents a specific case for $L = 2$. The resonant energy required for cyclotron interaction with MeV protons is plotted as a function of resonant latitude and frequency. We observe that the required energy of the target particles increases with latitude and decreases with frequency, which means that compared to resonance at higher latitudes, interaction at the equator (longer resonance times, higher scattering) for a fixed target's energy would require lower frequencies.

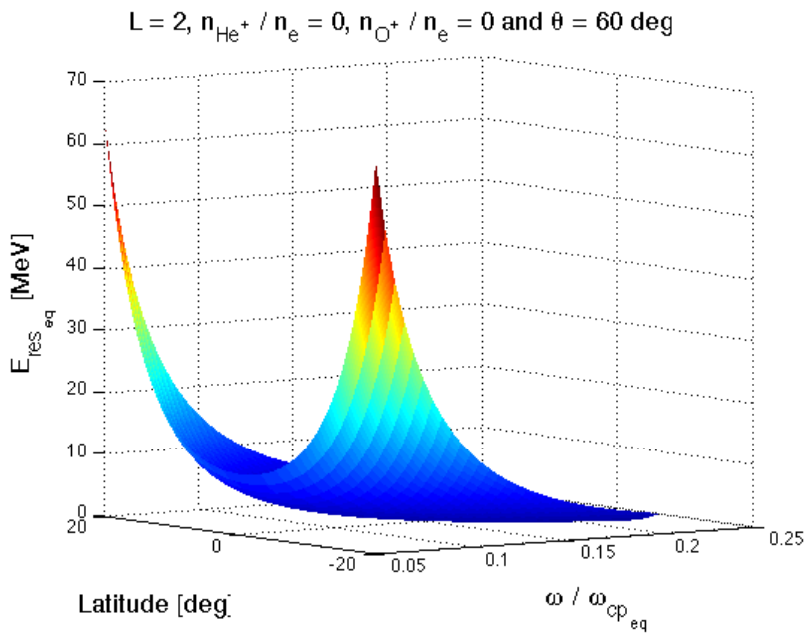

Figure 4.12: Resonant energy of protons for EMIC interaction versus resonant latitude and frequency

Similar to Inan's studies for the whistler-electron case [50], we have analyzed the interaction of parallel propagating EMIC waves and a single sheet of protons uniformly distributed in Larmor phase. Figure 4.13 represents the RMS scattering referred to the equator versus the wave power flux for equatorial interaction between protons at the edge of the loss cone and parallel propagating EMIC waves at $L = 1.5$. This analysis is useful because it shows the importance of the wave field term compared to the basic geomagnetic field in the variation of the phase η defined in Eq. 3.42. This wave term has been neglected in our derivation of the equations of motion for interaction with oblique EMIC waves (Eq. 3.52), but it has been included in this study of parallel propagation following the formulation in [50]. According to these results and for the given parameters, the wave field is proportional to the scattering for power fluxes $\leq 10^{-4} W/m^2$; in the literature this regime is called "linear mode", where the wave term in the equation for $\dot{\eta}$ can be neglected. This linear mode is equivalent to assume that the wave effects are so small that the variation of η is very close to what it would have been without wave.

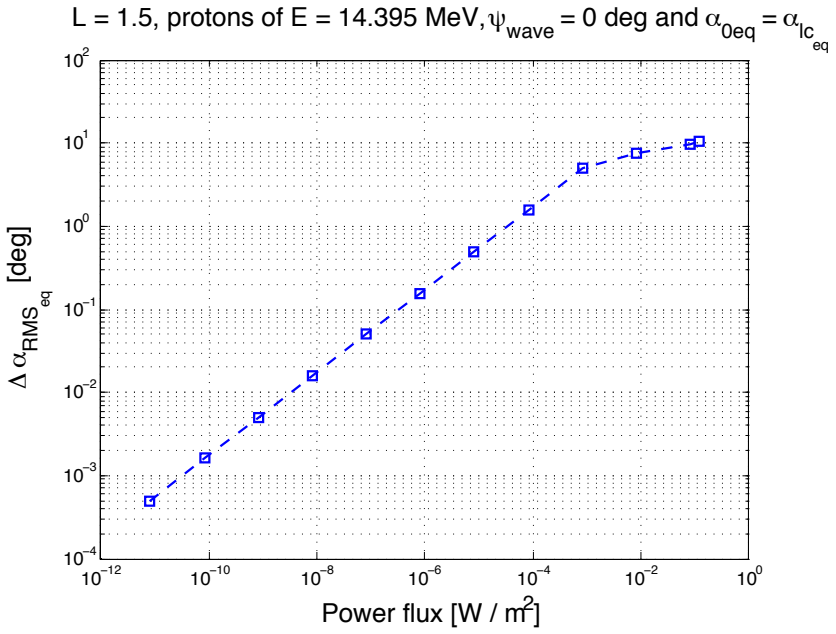

Figure 4.13: RMS pitch-angle scattering versus power flux for parallel EMIC-proton resonant interaction at the equator ($L = 1.5$)

According to these results and neglecting the wave term in the phase equation, Figure 4.14 presents the pitch-angle scattering referred to the equator versus latitude of a single equatorially ($L = 1.5$) resonant sheet of protons interacting with an oblique EMIC wave with a wave-normal angle of $\psi = 80°$ and power flux of $8.1^{-6}W/m^2$. These protons have their velocity vector at the equator along the edge of the loss cone and are uniformly distributed in Larmor phase (each curve corresponds to a different phase). The RMS scattering for this case equals $\Delta\alpha_{RMS}|_{eq} = 0.06°$, which is one order of magnitude smaller than the scattering obtained for field aligned waves ($\Delta\alpha_{RMS}|_{eq} = 0.5°$) as shown in Figure 4.13. Finally, Figure 4.15 presents the maximum scattering of each of these protons in the sheet versus their initial Larmor phase. In this Figure we can perfectly observe the sinusoidal behavior of the scattering characteristic of this linear behavior. When neglecting the wave term from the phase equation, the variation in time of the parallel and perpendicular momentum (Eqs. 3.53 and 3.54) depend sinusoidally on the phase, where η is now non dependent on the wave field.

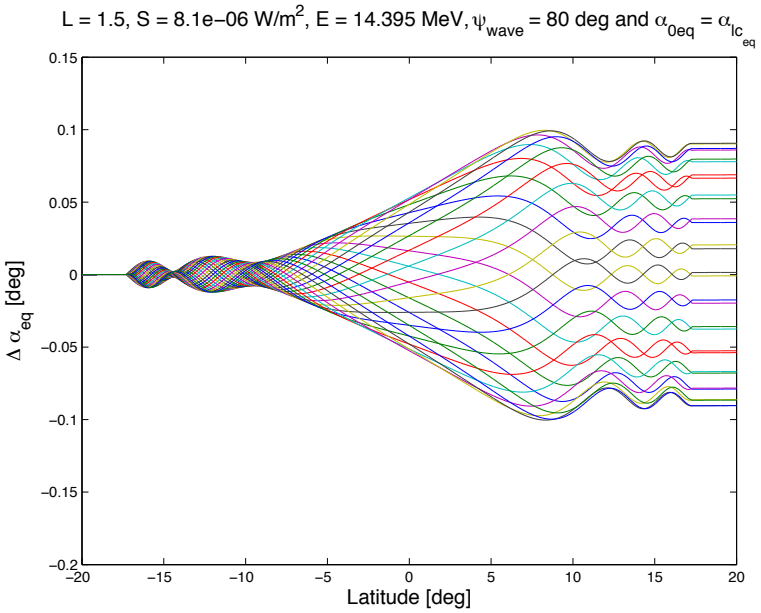

Figure 4.14: Total pitch-angle scattering versus latitude for a oblique EMIC wave interacting with equatorially resonant protons ($L = 1.5$)

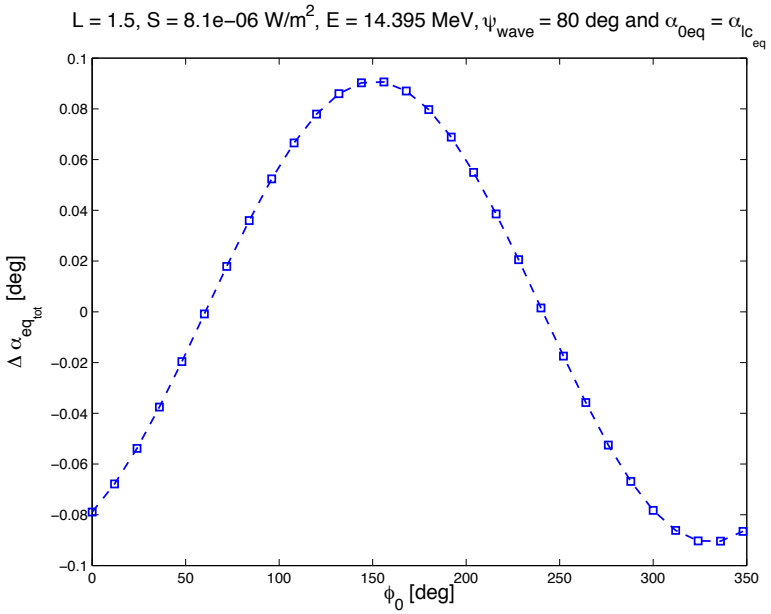

Figure 4.15: Maximum pitch-angle scattering versus initial Larmor phase for a oblique EMIC wave interacting with equatorially resonant protons ($L = 1.5$)

Chapter 5

Future Work and Proposed Schedule

The future tasks described along this proposal and their planning are summarized in Figure 5.1:

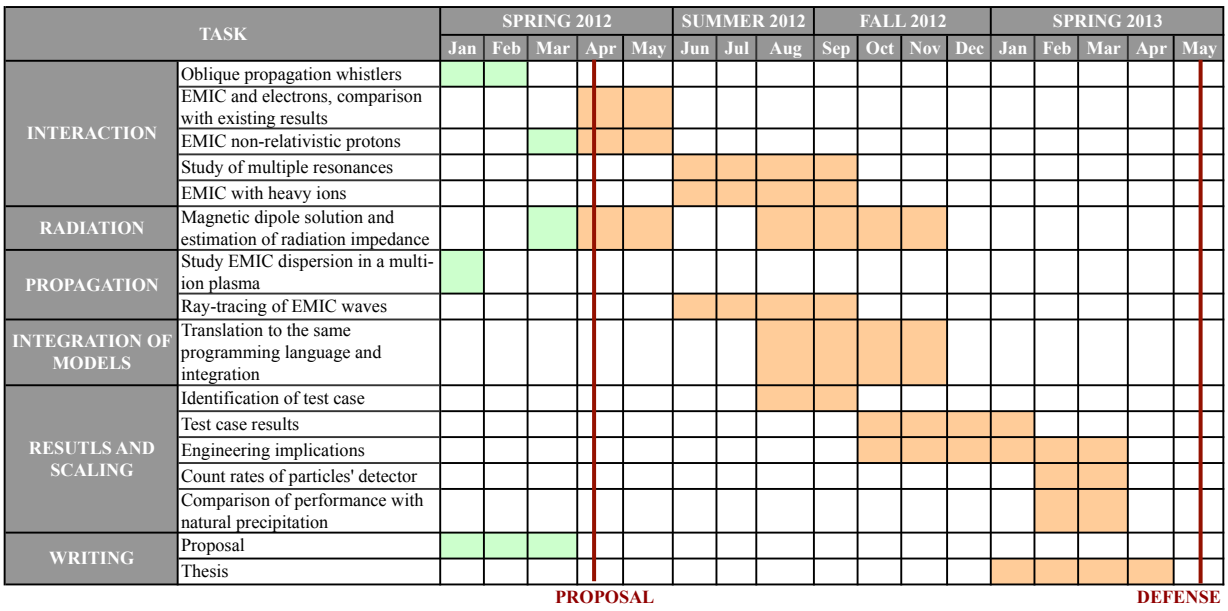

Figure 5.1: Tasks' planning

Bibliography

[1] B. Abel and R. M. Thorne. Electron scattering loss in earth's inner magnetosphere 1. Dominant physical processes. *Journal of Geophysical Research*, 103(A2):2385–2396, 1998.

[2] J. M. Albert. Cyclotron resonance in an inhomogeneous magnetic field. *Physics of Fluids B: Plasma Physics*, 5:2744, 1993.

[3] J. M. Albert. Analysis of quasi-linear diffusion coefficients. *Journal of Geophysical Research*, 104(A2):2429–2441, 1999.

[4] J. M. Albert. Gyroresonant interactions of radiation belt particles with a monochromatic electromagnetic wave. *Journal of Geophysical Research*, 105(A9):21191–21209, 2000.

[5] J. M. Albert. Nonlinear interaction of outer zone electrons with VLF waves. *Geophys. Res. Lett.*, 29(8), 04 2002.

[6] J. M. Albert. Evaluation of quasi-linear diffusion coefficients for EMIC waves in a multispecies plasma. *Journal of Geophysical Research*, 108, 06 2003.

[7] J. M. Albert. Evaluation of quasi-linear diffusion coefficients for whistler mode waves in a plasma with arbitrary density ratio. Technical report, DTIC Document, 2005.

[8] J. M. Albert and J. Bortnik. Nonlinear interaction of radiation belt electrons with electromagnetic ion cyclotron waves. *Geophysical Research Letter*, 36, 06 2009.

[9] B. J. Anderson. Recent observations of electromagnetic ion cyclotron waves in space. *Advances in Space Research*, 17(10):41–50, 1996.

[10] B. J. Anderson, R. E. Erlandson, and L. J. Zanetti. A statistical study of Pc 1-2 magnetic pulsations in the equatorial magnetosphere, 2. Wave properties. *Journal of Geophysical Research*, 97(A3):3089–3101, 1992.

[11] J. J. Angerami and J. O. Thomas. Studies of Planetary Atmospheres 1. The Distribution of Electrons and Ions in the Earth's Exosphere. *Journal of Geophysical Research*, 69(21):4537–4560, 1964.

[12] M. Ashour-Abdalla. Amplification of whistler waves in the magnetosphere. *Planetary and Space Science*, 20(5):639 – 662, 1972.

[13] D. N. Baker. The occurrence of operational anomalies in spacecraft and their relationship to space weather. *Plasma Science, IEEE Transactions on*, 28(6):2007–2016, 2000.

[14] D. N. Baker, R. D. Belian, P. R. Higbie, R. W. Klebesadel, and J. B. Blake. Deep dielectric charging effects due to high-energy electrons in Earth's outer magnetosphere. *Journal of electrostatics*, 20(1):3–19, 1987.

[15] K. Balmain. The impedance of a short dipole antenna in a magnetoplasma. *IEEE Transactions on Antennas and Propagation*, 12(5):605–617, September 1964.

[16] T. F. Bell. The nonlinear gyroresonance interaction between energetic electrons and coherent VLF waves propagating at an arbitrary angle with respect to the Earth's magnetic field. *Journal of Geophysical Research*, 89:905–918, 1984.

[17] T. F. Bell, U. S. Inan, and T. Chevalier. Current distribution of a VLF electric dipole antenna in the plasmasphere. *Radio Science*, 41(2), 04 2006.

[18] T. F. Bell, U.S. Inan, J. Bortnik, and J. D. Scudder. The landau damping of magnetospherically reflected whistlers within the plasmasphere. *Geophysical research letters*, 29(15):23–1, 2002.

[19] T. F. Bell and T. Wang. Radiation resistance of a small filamentary loop antenna in a cold multicomponent magnetoplasma. *IEEE Transactions on Antennas and Propagation*, 19(4):517–522, 1971.

[20] J. Bortnik, U. S. Inan, and T. F. Bell. Temporal signatures of radiation belt electron precipitation induced by lightning-generated MR whistler waves: 1. Methodology. *Journal of Geophysical Research*, 111, 2006.

[21] W. L. Brown and J. D. Gabbe. The electron distribution in the Earth's radiation belts during July 1962 as measured Telstar. *Journal of Geophysical Research*, 68(3):607–618, 1963.

[22] K.G. Budden. *Radio waves in the ionosphere*. Cambridge University Press, 1966.

[23] H. C. Chang. *Cyclotron Resonant Scattering of Energetic Electrons by Electromagnetic Waves in the Magnetosphere*. PhD thesis, Stanford University, 09/1983 1983.

[24] H. C. Chang and U. S. Inan. Quasi-relativistic electron precipitation due to interactions with coherent VLF waves in the magnetosphere. *Journal of Geophysical Research*, 88:318–328, 1983.

[25] H. C. Chang and U. S. Inan. Lightning-induced electron precipitation from the magnetosphere. *Journal of Geophysical Research*, 90:1531–1541, 1985.

[26] H. C. Chang and U. S.. Inan. Test particle modeling of wave-induced energetic electron precipitation. *Journal of Geophysical Research*, 90:6409–6418, 1985.

[27] T. W. Chevalier, U. S. Inan, and T. F. Bell. Fluid simulation of the collisionless plasma sheath surrounding an electric dipole antenna in the inner magnetosphere. *Radio Science*, 45:1010, feb 2010.

[28] T. W. Chevalier, U. S. Inan, and T. F.F. Bell. Terminal impedance and antenna current distribution of a VLF electric dipole in the inner magnetosphere. *Antennas and Propagation, IEEE Transactions on*, 56(8):2454 –2468, 2008.

[29] D. Cohen, G. Spanjers, J. Winter, G. Ginet, B. Dichter, A. Adler, and M. Tolliver. Design and Systems Engineering of AFRL's Demonstration and Sciences Experiment. 2005.

[30] A. C. Das. A mechanism for VLF emissions. *Journal of Geophysical Research*, 73(23):7457–7471, 1968.

[31] M. De Soria-Santacruz. Radiation of VLF/ELF waves from a magnetospheric tether. Master's thesis, Massachusetts Institute of Technology, June 2011.

[32] K. Dobes. The HM wave-particle cyclotron resonance for non-parallel propagation. *Planetary and Space Science*, 18(3):395 – 406, 1970.

[33] R. E. Erlandson and A. J. Ukhorskiy. Observations of electromagnetic ion cyclotron waves during geomagnetic storms: Wave occurrence and pitch angle scattering. *Journal of Geophysical Research*, 106(A3):3883–3895, 2001.

[34] B. J. Fraser. Observations of ion cyclotron waves near synchronous orbit and on the ground. *Space Science Reviews*, 42(3):357–374, 1985.

[35] B. J. Fraser, J. C. Samson, Y. D. Hu, R. L. McPherron, and C. T. Russell. Electromagnetic ion cyclotron waves observed near the oxygen cyclotron frequency by ISEE 1 and 2. *Journal of Geophysical Research*, 97(A3):3063–3074, 1992.

[36] B. J. Fraser, H. J. Singer, W. J. Hughes, J. R. Wygant, R. R. Anderson, and Y. D. Hu. CRRES Poynting vector observations of electromagnetic ion cyclotron waves near the plasmapause. *Journal of Geophysical Research*, 101(A7):15331–15, 1996.

[37] G. P. Ginet and J. M. Albert. Test particle motion in the cyclotron resonance regime. *Physics of Fluids B: Plasma Physics*, 3:2994, 1991.

[38] G. P. Ginet and M. A. Heinemann. Test particle acceleration by small amplitude electromagnetic waves in a uniform magnetic field. *Physics of Fluids B: Plasma Physics*, 2:700, 1990.

[39] G. P. Ginet, J. Stuart, A. Adler, D. Smith, M. Scherbarth, et al. AFRL's Demonstration and Science Experiments (DSX) Mission. In *Proceedings of SPIE*, 2009.

[40] S. A. Glauert and R. B. Horne. Calculation of pitch angle and energy diffusion coefficients with the PADIE code. *Journal of Geophysical Research*, 110(A4), 04 2005.

[41] L. Gomberoff and R. Neira. Convective Growth Rate of Ion Cyclotron Waves in a H+-He+ and H+-He+-O+ Plasma. *Journal of Geophysical Research*, 88(A3):2170–2174, 1983.

[42] J. Haselgrove. Ray theory and a new method for ray tracing. In *Physics of the Ionosphere*, volume 1, page 355, 1955.

[43] R. J. Hastie, J. B. Taylor, and F. A. Haas. Adiabatic invariants and the equilibrium of magnetically trapped particles. *Annals of Physics*, 41(2):302–338, 1967.

[44] R. B. Horne and R. M. Thorne. On the preferred source location for the convective amplification of ion cyclotron waves. *Journal of Geophysical Researchesearch*, 98(A6):9233–9247, 1993.

[45] R. B. Horne and R. M. Thorne. Relativistic electron acceleration and precipitation during resonant interactions with whistler-mode chorus. *Geophysical Research Letters*, 30(10):1527, 2003.

[46] J. L. Horwitz, R. H. Comfort, P.G. Richards, M.O. Chandler, C.R. Chappell, P. Anderson, W. B Hanson, and L. H. Brace. Plasmasphere-ionosphere coupling, 2. Ion composition measurements at plasmaspheric and ionospheric altitudes and comparison with modeling results. *Journal of Geophysical Research*, 95(A6):7949–7959, 1990.

[47] Y. D. Hu and B. J. Fraser. Group travel time of EM waves with frequencies near the ion cyclotron frequency in the two-ion magnetosphere. *Australian journal of physics*, 45(5):695–716, 1992.

[48] N. D. Hulkower and R. J. Rusch. Study of Plasma Motor Generator (PMG) tether system for orbit reboost. 1987.

[49] W. L. Imhof, J. B. Reagan, H. D. Voss, E. E. Gaines, D. W. Datlowe, J. Mobilia, R. A. Helliwell, U. S. Inan, J. Katsufrakis, and R.G. Joiner. Direct observation of radiation belt electrons precipitated by the controlled injection of VLF signals from a ground-based transmitter. *Geophysical Research Letters*, 10:361–364, 1983.

[50] U. S. Inan. *Non-linear gyroresonant interactions of energetic particles and coherent VLF waves in the magnetosphere*. Ph. d thesis, Stanford University, 1977.

[51] U. S. Inan. Gyroresonant pitch angle scattering by coherent and incoherent whistler mode waves in the magnetosphere. *Journal of Geophysical Research*, 92:127–142, 1987.

[52] U. S. Inan and T. F. Bell. The plasmapause as a vlf wave guide. *Journal of Geophysical Research*, 82(19):2819, 1977.

[53] U. S. Inan and T. F. Bell. Pitch angle scattering of energetic particles by oblique whistler waves. *Geophysical Research Letters*, 18:49–52, 1991.

[54] U. S. Inan, T. F. Bell, and J. Bortnik. Controlled precipitation of radiation belt electrons. *Journal of Geophysical Research*, 108(A5), 2003.

[55] U. S. Inan, T. F. Bell, and H. C. Chang. Particle precipitation induced by short-duration VLF waves in the magnetosphere. *Journal of Geophysical Research*, 87:6243–6264, 1982.

[56] U. S. Inan, T. F. Bell, and R. A. Helliwell. Nonlinear pitch angle scattering of energetic electrons by coherent VLF waves in the magnetosphere. *Journal of Geophysical Research*, 83(A7):3235–3253, 1978.

[57] U. S. Inan, H. C. Chang, and R. A. Helliwell. Electron precipitation zones around major ground-based VLF signal sources. *Journal of Geophysical Research*, 89(A5):2891–2906, May 1984.

[58] U. S. Inan, F. Knifsend, and J. Oh. Subionospheric VLF 'imaging' of lightning-induced electron precipitation from the magnetosphere. *Journal of Geophysical Research*, 95:17217–17231, 1990.

[59] U. S. Inan and S. Tkalcevic. Nonlinear equations of motion for Landau resonance interactions with a whistler mode wave. *Journal of Geophysical Research*, 87:2363–2367, 1982.

[60] V. K. Jordanova, C. J. Farrugia, J. M. Quinn, R. M. Thorne, K. E Ogilvie, R. P. Lepping, G. Lu, A. J. Lazarus, M. F. Thomsen, and R. D. Belian. Effect of wave-particle interactions on ring current evolution for January 10-11, 1997: Initial results. *Geophysical Research Letter*, 25.

[61] V. K. Jordanova, C. J. Farrugia, R. M. Thorne, G. V. Khazanov, G. D. Reeves, and M. F. Thomsen. Modeling ring current proton precipitation by electromagnetic ion cyclotron waves during the May 14–16, 1997, storm. *Journal of Geophysical Research*, 106.

[62] V. K. Jordanova, J. U. Kozyra, and A. F. Nagy. Effects of heavy ions on the quasi-linear diffusion coefficients from resonant interactions with electromagnetic ion cyclotron waves. *Journal of Geophysical Research*, 101(A9):19771–19778, September 1996.

[63] V. K. Jordanova, J. U. Kozyra, A. F. Nagy, and G. V. Khazanov. Kinetic model of the ring current-atmosphere interactions. *Journal of Geophysical Research*, 102.

[64] Adolph S. Jursa, editor. *Handbook of geophysics and the space environment*. Air Force Research Laboratory, US Air Force, Fourth edition, 1985.

[65] C. Kennel and H. Petschek. Limit on stably trapped particle fluxes. *Journal of Geophysical Research*, 71(1):1–28, 1966.

[66] C. F. Kennel and F. Engelmann. Velocity space diffusion from weak plasma turbulence in a magnetic field. *Physics of Fluids*, 9(12):2377, 1966.

[67] G. V. Khazanov and K. V. Gamayunov. Effect of EMIC wave normal angle distribution on relativistic electron scattering in outer RB. Technical report, NASA.

[68] G. V. Khazanov, K. V. Gamayunov, D. L. Gallagher, and J. U. Kozyra. Self-consistent model of magnetospheric ring current and propagating electromagnetic ion cyclotron waves: Waves in multi-ion magnetosphere. *Journal of Geophysical Research*, 111(A10), 10 2006.

[69] G. V. Khazanov, K. V. Gamayunov, V. K. Jordanova, and E. N. Krivorutsky. A self-consistent model of the interacting ring current ions and electromagnetic ion cyclotron waves, initial results: Waves and precipitating fluxes. *Journal of Geophysical Research*, 107(A6), 06 2002.

[70] GV Khazanov, KV Gamayunov, DL Gallagher, JU Kozyra, and MW Liemohn. Self-consistent model of magnetospheric ring current and propagating electromagnetic ion cyclotron waves: 2. wave-induced ring current precipitation and thermal electron heating. *J. Geophys. Res*, 112:A04209, 2007.

[71] H. C. Koons, B. C. Edgar, and A. L. Vampola. Precipitation of inner zone electrons by whistler mode waves from the VLF transmitters UMS and NWC. *Journal of Geophysical Research*, 86(A2):640–648, 1981.

[72] H. H. Kuehl. Electromagnetic radiation from an electric dipole in a cold anisotropic plasma. *Physics of Fluids*, 5(9):1095–1104, 1962.

[73] P. Kulkarni, U. S. Inan, and T. F. Bell. Energetic electron precipitation induced by space based VLF transmitters. *Journal of Geophysical Research*, 113, 2008.

[74] W. Li, Y. Y. Shprits, and R. M. Thorne. Dynamic evolution of energetic outer zone electrons due to wave-particle interactions during storms. *J. Geophys. Res.*, 112(A10), 10 2007.

[75] K. R. Lorentzen, M. P. McCarthy, G. K. Parks, J. E. Foat, R. P. Lin, R. M. Millan, D. M. Smith, and J. P. Treilhou. Precipitation of relativistic electrons by interaction with electromagnetic ion cyclotron waves. *Journal of Geophysical Research-Space Physics*, 105(A3):5381–5389, 2000.

[76] T. M. Loto'aniu, B. J. Fraser, and C. L. Waters. Propagation of electromagnetic ion cyclotron wave energy in the magnetosphere. *Journal of Geophysical Research*, 110, 07 2005.

[77] G. R. Ludlow. Growth of obliquely propagating ion cyclotron waves in the magnetosphere. *Journal of Geophysical Research*, 94(A11):15385–15391, November 1989.

[78] L. R. Lyons. General relations for resonant particle diffusion in pitch angle and energy. *Journal of Plasma Physics*, 12(01):45–49, 1974.

[79] L. R. Lyons. Pitch angle and energy diffusion coefficients from resonant interactions with ion–cyclotron and whistler waves. *Journal of Plasma Physics*, 12(03):417–432, 1974.

[80] L. R. Lyons and R. M. Thorne. Parasitic pitch angle diffusion of radiation belt particles by ion cyclotron waves. *Journal of Geophysical Research*, 77(28), October 1972.

[81] L. R. Lyons, R. M. Thorne, and C. F. Kennel. Pitch-angle diffusion of radiation belt electrons within the plasmasphere. *Journal of Geophysical Research*, 77(19):3455–3474, 1972.

[82] L. R. Lyons and D. J. Williams. The quiet time structure of energetic (35-560 keV) radiation belt electrons. *Journal of Geophysical Research*, 80(7):943–950, 1975.

[83] N. P. Meredith, R. M. Thorne, R. B. Horne, D. Summers, B. J. Fraser, and R. R. Anderson. Statistical analysis of relativistic electron energies for cyclotron resonance with EMIC waves observed on CRRES. *Journal of Geophysical Research*, 108, 06 2003.

[84] Y. Miyoshi, K. Sakaguchi, K. Shiokawa, D. Evans, J. Albert, M. Connors, and V. Jordanova. Precipitation of radiation belt electrons by EMIC waves, observed from ground and space. *Geophysical Research Letter*, 35, 12 2008.

[85] F. S. Mozer, D. D. Elliott, J. D. Mihalov, G. A. Paulikas, A. L. Vampola, and S. C. Freden. Preliminary analysis of the fluxes and spectrums of trapped particles after the nuclear test of July 9, 1962. *Journal of Geophysical Research*, 68(3):641–649, 1963.

[86] NASA. AE-8/AP-8 Radiation Belt Models.

[87] NASA Data Center National Space Science. Intercosoms 24, March 2012.

[88] T. G. Northrop. Adiabatic charged-particle motion. *Reviews of Geophysics*, 1(3):283–304, 1963.

[89] T. G. Northrop and E. Teller. Stability of the adiabatic motion of charged particles in the earth's field. *Physical Review*, 117(1):215, 1960.

[90] G. F. Pieper. A second radiation belt from the July 9, 1962, nuclear detonation. *Journal of Geophysical Research*, 68(3):651–655, 1963.

[91] J. L. Rauch and A. Roux. Ray tracing of ULF waves in a multicomponent magnetospheric plasma: Consequences for the generation mechanism of ion cyclotron waves. *Journal of Geophysical Research*, 87(A10):8191–8198, 1982.

[92] J. L. Ristic-Djurovic. *Gyroresonant scattering of radiation belt electrons by oblique whistler waves.* Ph. d thesis, Stanford University, May 1993.

[93] J. L. Ristic-Djurovic, U. S. Inan, and T. F. Bell. Precipitation of suprathermal(100 ev) electrons by oblique whistler waves. *Geophysical research letters*, 19(16):1639–1642, 1992.

[94] C. J. Rodger, M. A. Clilverd, Th. Ulich, P. T. Verronen, E. Turunen, and N. R. Thomson. The atmospheric implications of radiation belt remediation. *Ann. Geophys.*, 24:2025–2041, 2006.

[95] C. J. Rodger, T. Raita, M. A. Clilverd, A. Seppälä, S. Dietrich, N. R. Thomson, and T. Ulich. Observations of relativistic electron precipitation from the radiation belts driven by EMIC waves. *Geophysical Research Letter*, 35, 08 2008.

[96] J. Schoenberg. The Demonstration and Science Experiments (DSX): A Fundamental Science Research Mission Advancing Technologies that Enable MEO Spaceflight. Technical report, DTIC Document, 2006.

[97] R. S. Selesnick, M. D. Looper, and R. A. Mewaldt. A theoretical model of the inner proton radiation belt. *Space Weather*, 5(4), 04 2007.

[98] D. R. Shklyar. Particle interaction with an electrostatic VLF wave in the magnetosphere with an application to proton precipitation. *Planetary and Space Science*, 34(11):1091 – 1099, 1986.

[99] DR Shklyar. Mechanism for proton precipitation triggered by a VLF wave injected into the magnetosphere. *JETP Letters*, 41:448–451, 1985.

[100] P. Song, B. W. Reinisch, V. Paznukhov, G. Sales, D. Cooke, J. N. Tu, X. Huang, K. Bibl, and I. Galkin. High-voltage antenna-plasma interaction in whistler wave transmission: Plasma sheath effects. *Journal of Geophysical Research*, 112(A3), March 2007.

[101] G. Spanjers, J. Winter, D. Cohen, A. Adler, J. Guarnieri, M. Tolliver, G. Ginet, B. Dichter, and J. Summers. The AFRL demonstration and science experiments (DSX) for DoD space capability in the MEO. In *Aerospace Conference, 2006 IEEE*, pages 10–pp. IEEE, 2006.

[102] R. L. Stenzel. Self-ducting of large-amplitude whistler waves. *Phys. Rev. Lett.*, 35(9):574–577, Sep 1975.

[103] R. L. Stenzel. Antenna radiation patterns in the whistler wave regime measured in a large laboratory plasma. *Radio Science*, 11(12):1045–1056, 1976.

[104] T. H. Stix. *Waves in Plasmas*. Springer-Verlag New York, Inc., 1992.

[105] D. Summers. Quasi-linear diffusion coefficients for field-aligned electromagnetic waves with applications to the magnetosphere. *J. Geophys. Res.*, 110, 08 2005.

[106] D. Summers and R. M. Thorne. Relativistic electron pitch-angle scattering by electromagnetic ion cyclotron waves during geomagnetic storms. *Journal of Geophysical Research*, 108(A4):1143, April 2003.

[107] Y. Takiguchi. Emission of whistler waves from an ionospheric tether. Master's thesis, Massachusetts Institute of Technology, September 2009.

[108] X. Tao and J. Bortnik. Nonlinear interactions between relativistic radiation belt electrons and oblique whistler mode waves. *Nonlinear Processes in Geophysics*, 17:599–604, 2010.

[109] R. M. Thorne and R. B. Horne. Cyclotron absorption of ion-cyclotron waves at the bi-ion frequency. *Geophysical Research Lettersesearch letters*, 20(4):317–320, 1993.

[110] R. M. Thorne, R. B. Horne, V. K. Jordanova, J. Bortnik, and Glauert Sarah. Interaction of EMIC Waves with Thermal Plasma and Radiation Belt Particles. Technical report, 2006.

[111] R. M. Thorne and C. F. Kennel. Quasi-trapped vlf propagation in the outer magnetosphere. *Journal of Geophysical Research*, 72(3):857–870, 1967.

[112] J. Tu, P. Song, and B. W. Reinisch. Plasma sheath structures around a radio frequency antenna. *Journal of Geophysical Research*, 113(A7), 07 2008.

[113] J. A. Van Allen, G. H. Ludwig, E. C. Ray, and C. E. McIlwain. Observation of high intensity radiation by satellites 1958 alpha and gamma. *Jet Propulsion*, 28(9):588–592, 1958.

[114] D. L. Voss, A. Gunda, D. Carssow, T. Fritz, A. Mavretic, and J. Sullivan. Overview of the loss cone imager fixed sensor head instrument. In *Proceedings of SPIE*, volume 7438, page 743808, 2009.

[115] M. Walt. *Introduction to geomagnetically trapped radiation*, volume 1. 2005.

[116] T. Wang and T. Bell. VLF/ELF input impedance of an arbitrarily oriented loop antenna in a cold collisionless multicomponent magnetoplasma. *IEEE Transactions on Antennas and Propagation*, 20(3):394 – 398, may 1972.

[117] T. Wang and T. Bell. On input impedance of an arbitrarily oriented small loop antenna in a cold collisionless magnetoplasma. *IEEE Transactions on Antennas and Propagation*, 21(5):745–746, 1973.

[118] T. N. C. Wang and T. F. Bell. Radiation resistance of a short dipole immersed in a cold magnetoionic medium. *Radio Science*, 4(2):167–177, 1969.

[119] T. N. C. Wang and T. F. Bell. On VLF radiation resistance of an electric dipole in a cold magnetoplasma. *Radio Science*, 5(3):605–610, 1970.

[120] T. N. C. Wang and T. F. Bell. Electric dipole radiation at VLF in a uniform warm magnetoplasma. *Revue de Physique Appliquee*, 7(1):11–20, 1972.

[121] T. N. C. Wang and T. F. Bell. VLF/ELF Radiation Patterns of Arbitrarily Oriented Electric and Magnetic Dipoles in a Cold Lossless Multicomponent Magnetoplasma. *Journal of Geophysical Research*, 77(7):1174–1189, March 1972.

[122] A. G. Yahnin and T. A. Yahnina. Energetic proton precipitation related to ion-cyclotron waves. *Journal of Atmospheric and Solar-Terrestrial Physics*, 69(14):1690–1706, 10 2007.

[123] D. T. Young, S. Perraut, A. Roux, C. de Villedary, R. Gendrin, A. Korth, G. Kremser, and D. Jones. Wave-Particle Interactions near ΩHe+ Observed on GEOS 1 and 2, 1. Propagation of Ion Cyclotron Waves in He+-Rich Plasma. *Journal of Geophysical Research*, 86(A8):6755–6772, 1981.